U.S. DEPARTMENT OF COMMERCE
LUTHER H. HODGES, *Secretary*
WEATHER BUREAU
F. W. REICHELDERFER, *Chief*

RESEARCH PAPER NO. 44

Three-Dimensional Wind Flow and Resulting Precipitation in a Northern California Storm

VANCE A. MYERS AND GEORGE A. LOTT
Hydrometeorological Section, Hydrologic Services Division
U.S. Weather Bureau, Washington, D.C.

QC
852
.U55
no. 44

LIBRARY
N.O.A.A
U S Dept of Commerce

WASHINGTON, D.C.
AUGUST 1963

For sale by the Superintendent of Documents, U.S. Government Printing Office, Washington, D.C. 20402 - Price 35 cents

National Oceanic and Atmospheric Administration
Weather Bureau Research Papers

ERRATA NOTICE

One or more conditions of the original document may affect the quality of the image, such as:

Discolored pages
Faded or light ink
Binding intrudes into the text

This has been co-operative project between the NOAA Central Library and the Climate Database Modernization Program, National Climate Data Center (NCDC). To view the original document contact the NOAA Central Library in Silver Spring, MD at (301) 713-2607 x 124 or Library.Reference@noaa.gov.

HOV Services
Imaging Contractor
12200 Kiln Court
Beltsville, MD 20704-1387
January 22, 2008

Blank page retained for pagination

TABLE OF CONTENTS

	Page
I. INTRODUCTION	
Orographic wind models	1
Locale	2
Methodology	2
II. THE DECEMBER 1955 STORM	
Period of study	3
Data available	3
Compositing	4
III. KEYS TO THE WIND	
Summary	5
Geostrophic speed relation	5
Geostrophic direction relation	9
Increase of wind with height	9
Turning of wind with height	9
Tentative trajectories	9
Dynamic trajectories	10
The minimum energy method of computing speeds over a ridge	12
The Central Valley technique	12
IV. SURFACE WIND AND PRESSURE	
Sea level pressure	13
Surface winds	13
V. SYNTHETIC TEMPERATURE SOUNDINGS	15
VI. CONFINED FLOW IN THE CENTRAL VALLEY	
Central Valley problem	16
Central Valley cross sections	16
Results of cross-sectional analysis	18
VII. DYNAMIC COMPUTATION OF WIND SPEED	
Two-dimensional wind flow	18
Changes in method for three-dimensional flow	19
Other elements in dynamic computations	20
Application of dynamic computation method	21
Results of dynamic computation method	22
VIII. THE COMPUTATION OF PRECIPITATION	
Precipitation model	37
Air trajectories	37
Mechanics of precipitation computation	37
IX. PREDICTED VS. OBSERVED PRECIPITATION	
Distribution at the ground	42
Volume comparison	42
Variation of precipitation with elevation	43
Layer contribution to total precipitation	44
X. CONCLUSION	45
REFERENCES	46

Three-Dimensional Wind Flow and Resulting Precipitation in a Northern California Storm

VANCE A. MYERS AND GEORGE A. LOTT

Hydrometeorological Section, Hydrologic Services Div., U.S. Weather Bureau, Washington, D.C.

[Manuscript received January 25, 1963; revised April 22, 1963]

ABSTRACT

By careful consideration of the observed winds and with the aid of various empirical and dynamic relationships, a steady-state 3-dimensional wind flow is deduced over northern California for a 24-hour stormy period. The production (or evaporation) of precipitation elements is estimated for all parts of the flow, the surviving elements are followed down to the surface, and the resulting precipitation pattern is compared with the observed.

I. INTRODUCTION

OROGRAPHIC WIND MODELS

A knowledge of the quantity of precipitation falling on mountain watersheds is an important factor in water management. If the probable volume of water to fall, or even in the process of falling, can be foretold, an optimum balance between water storage needs and risk of overburdening the system can be more intelligently effected. Of equal concern with the forecasting problem is the design problem. The probable maximum precipitation over a basin above a dam site is taken into account in deciding on the safe capacity of the spillway. The more accurate the storm model evolved for a given region, the more confidence can be attached to extrapolations to probable maximum conditions.

The effort to explain rainfall over mountains leads inevitably to a hypothetical wind model. Rain is intimately related to wind and wind is not measured directly. Over the ridges and slopes of northern California, the locale of this study, there are no upper-wind observations and few surface observations. Nor are any other mountainous regions better equipped with observations.

Pockels [3] is the father of the earliest theoretical orographic rain wind flow model known to the authors. He applied the techniques of classical hydrodynamics and assumed a steady-state frictionless two-dimensional laminar flow across a ridge of prescribed geometric form, capped at some great height by horizontal flow of constant velocity. Bjerknes [1] calculated rates of precipitation from layers of adiabatically ascending air, using the equation of continuity and an arbitrary exponential decrease of vertical component of wind with height. From the implied wind field (in two dimensions) trajectories of raindrops were computed and accumulated depths compared with the observed in the March 2, 1938 storm over the Sierra Madres of California. In *Hydrometeorological Report No. 21A* of the Weather Bureau [4], concerned with probable maximum precipitation in the Los Angeles area, a simple two-dimensional model was evolved which used pressure rather than height as the vertical coordinate, thereby

eliminating the complication of variation of density with height and simplifying in concept and practice, the use of continuity of mass. The inflow wind in a vertical plane was estimated from pilot balloon observations or from the geostrophic wind; the outflow wind in a vertical plane over a downstream barrier was computed from the equation of continuity. This model was applied to the San Joaquin Valley in *Hydrometeorological Report No. 24* [5] and was also employed in some other studies.

The next advance is found in later studies of probable maximum precipitation in California [6], in which the two-dimensional flow is subdivided into layers, an allowance is made for friction, and a theory is developed for computing, rather than arbitrarily assigning, the height (or pressure) of the "nodal surface" of approximately horizontal flow. This latter theory has been described by one of the authors of this report [2].

The intended contribution of the present report is to depart from more than a half century of two-dimensional orographic flow models and to begin the development of a three-dimensional model. The two-dimensional model should give fairly reliable results if the currents at the various levels are not too dissimilar in direction. In mountainous regions, however, the low-level air is generally channeled by the ridges. As a result, the surface air may flow in a direction widely different from the direction of flow at upper levels. A basin presenting an upslope aspect to this low-level current may receive much more rain than another basin on the same general ridge with a different local configuration of the terrain. The two-dimensional model offers no basis for evaluating this difference.

Knowledge of the three-dimensional airflow is also necessary in order to determine where the condensation products strike the ground since the fall time is appreciable.

LOCALE

The region studied, California north of 37° 30′ N., was chosen for several reasons. First, the topography here, in its grosser aspects, is relatively uncomplicated consisting of the Coast Range facing the sea, continuous except at the Golden Gate, the higher parallel Sierra Nevada, and the flat near-sea-level floor of the Sacramento Valley between. Second, there is relative constancy of wind direction in precipitation storms in this area. Third, this is a region in which there is a great interest in the conservation and use of water resources and vast expenditures over several decades are planned. Therefore, any clue to the behavior of precipitation storms here may have considerable economic benefit.

METHODOLOGY

The method of attack on this problem has been to derive mutually consistent three-dimensional fields of wind, temperature, pressure, moisture, and precipitation for a selected storm period. A further logical step would be, in turn, to analyze several different storms. In view of the formidable labor involved this lay beyond the scope of the present investigation. The work plan was to find a flow that was compatible with all the available observations and which conformed to whatever dynamic principles could be brought to bear.

The first starting point was the input along the coast during the selected storm. Fields of inflow wind, pressure, temperature, and moisture were constructed in a manner to be explained. This flow was then carried by dynamic computations, using an electronic computer, across the Coast Range, the Central Valley, and up the westward slope of the Sierra Nevada. The minimum energy method of Myers [2] was used to solve for the wind speed (but not the wind direction), the pressure, and the temperature. The wind direction variation near the ground was based on empirical studies and at higher levels on both empirical and dynamic trajectories.

The second starting point was a carefully constructed sea level pressure map. With this chart as a base, preliminary constant pressure charts at selected levels up to 300 mb. were prepared using all available techniques to augment observed data. Heights on the constant pressure charts were both input to and output from the cross-mountain dynamic computations. The whole interrelated complex of factors applied in the study is shown diagrammatically in figure 4*a–c*.

Second approximations were made where needed in the various stages of computation. For example, upper-level temperatures were assumed in regions of no observations in order to compute the upper-level constant pressure charts on which, in turn, upper-level winds were based in part. Advection of temperature from the coastal input with these winds did not yield exactly the

assumed temperatures at all interior points, thus requiring a second round of computation.

Finally, when a three-dimensional wind field consistent with pressures and temperatures was obtained, the condensation resulting from adiabatic cooling was computed by layers roughly 100 mb. in thickness. The trajectory of fall of the precipitation elements to the ground was taken into account by letting the snowflakes and raindrops drift forward with the determined wind field while falling at an assumed terminal speed.

In the original work plan it was intended to treat the observed precipitation as an important part of the observational material and to adjust the wind field to take care of significant differences between observed and computed orographic precipitation. This was not done except in one small area because the differences between computed precipitation (prepared without reference to the observed) and observed precipitation were explainable by (a) the necessary over-simplification of topography for computational purposes from its true rugged character; (b) the assumption of laminar flow neglecting convection; and (c) the random variations to be expected in this kind of study. A forced fit of the observed and computed precipitation was regarded as artificial and not leading to a more probable wind field. In one area, near Mt. Shasta, one additional trajectory was computed after comparison of computed and observed precipitation to increase the detail on the computed chart.

II. THE DECEMBER 1955 STORM

PERIOD OF STUDY

The most widespread and severe floods of the past 100 years in northern California occurred in December 1955. The heaviest rain in the storm was in the three days, December 21–23, 1955. During this 3-day period two extremely heavy bursts of rain occurred, the first centered late on the 21st and the second early on the 23d. The winds were stronger during the second burst but the precipitation was somewhat lighter, because of a lower moisture content of the air, especially above 700 mb. The period chosen for study was the 24 hours ending 0400 PST of the 22d (25 consecutive hourly observations), when a quasi-steady-state condition existed in the wind, temperature, and pressure over northern and central California. The surface weather chart near the middle of the study period is depicted in figure 1. This is the same period used by one of the authors [2] in the previously cited two-dimensional analysis of wind flow over the Sierra Nevada downwind from Sacramento.

DATA AVAILABLE

Surface. Photocopies of original surface observations including barograph traces were obtained for all weather reporting stations in California north of about 37° and for adjacent areas of Oregon and Nevada. The majority of stations reported hourly. Hourly pressures were obtained at all stations by recourse to the barograms. The names and positions of these land surface stations can be seen on figure 2. Some ship reports were also available but are not shown on the figure.

Upper air. Radiosonde observations available in the storm study area and period include Oakland and Merced, Calif., and Medford, Oreg. Raob stations farther afield were Portland, Oreg.; Boise, Idaho; Ely and Las Vegas, Nev.; and Santa Maria, Pt. Mugu, Inyokern (China Lake), and Los Angeles, Calif. This latter group of stations was of little direct value except for orienting lines at the edges of the maps. The radiosonde at ship N, (30° N. 140° W.), although far off the coast, was useful for estimating upper-air moisture because of its upwind position.

Winds aloft observations in the study area were taken at Oakland, Sacramento, Reno, Red Bluff, Medford, and Merced. Those at Oakland and Merced and some of those at Medford were rawins and so extended to greater heights than

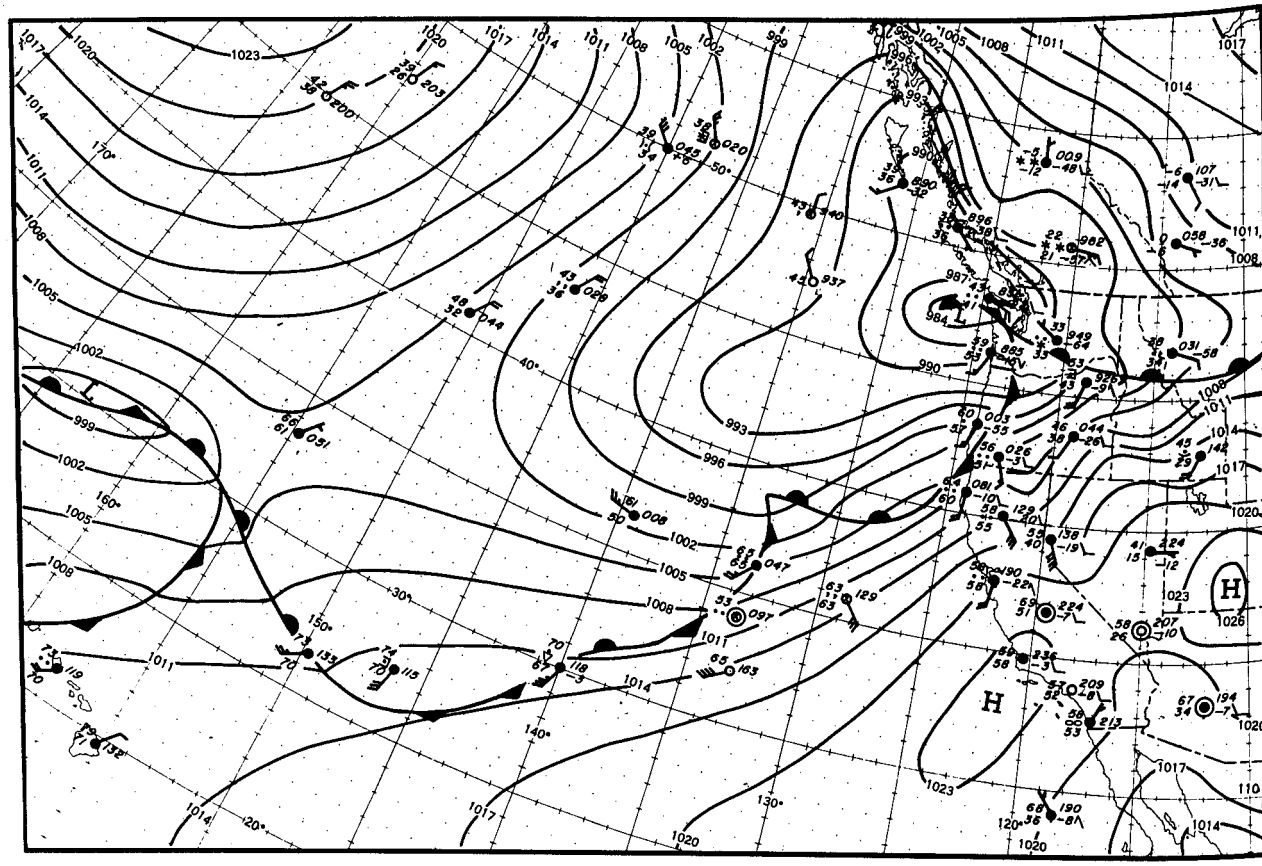

FIGURE 1.—Surface weather map, northeastern Pacific area, 1630 PST, December 21, 1955, about the middle of the 24-hour period used for study in this report. During the period December 21–23, two heavy bursts of rainfall occurred in northern California, the first centered late on the 21st and the second early on the 23d.

the others which depend on visual contact with the sounding balloon.

COMPOSITING

Data for the 24-hour study period were composited. The purpose of compositing, rather than analyzing at particular observational times, was to highlight the fixed orographic controls of the flow and to smooth out, to some extent, transient phenomena related more to a moving weather system than to the terrain.

The sea level and surface data over the storm area were composited by averaging the 25 individual hourly observations. If a station did not report for a particular hour, an estimate of its pressure, temperature, and dew point was obtained from an individual hourly map (not reproduced in this report). The hourly maps were also used to develop constant correction to the sea level pressures at several stations to bring them into line with the general pattern. However, interpolations were not made for surface winds, since wind speed and direction are more variable than the other elements. The surface winds were, therefore, composited using the total number of observations available.

The sea level isobars were constructed over the Pacific Ocean by means of an auxiliary composite sea level chart (not shown) made from National Meteorological Center 6-hourly Northern Hemisphere surface maps. A small pressure correction to the over-sea isobars was necessary in order to make the sea isobars averaged from 5 observation times compatible with the land isobars averaged from 25 observation times. This correction of less than 1 mb. was worked out by averaging coastal stations both ways.

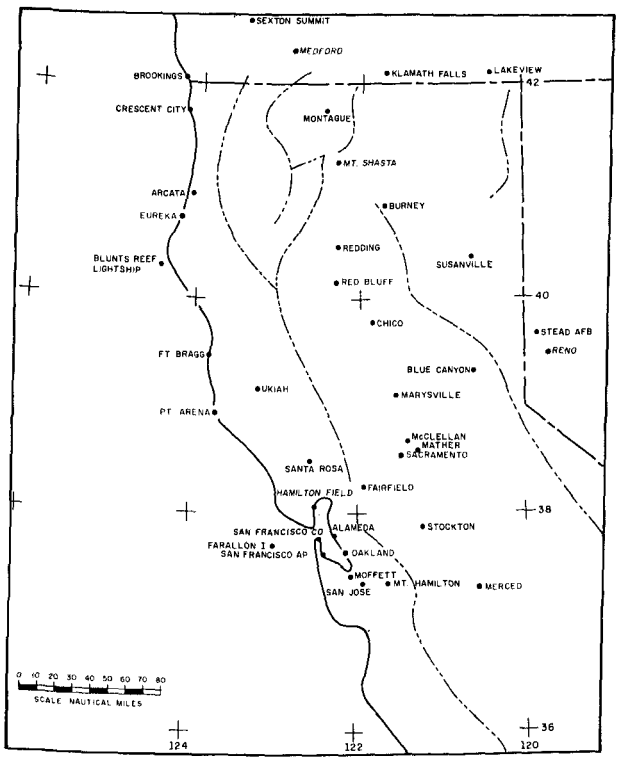

FIGURE 2.—The surface observational network.

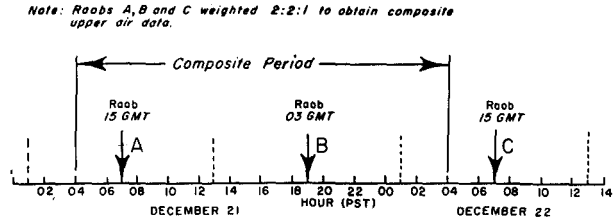

FIGURE 3.—Time cross section showing the hourly surface observations which were averaged for the study (0400 to 0400 PST) and the relation of the available raob soundings to these.

The soundings, and therefore the upper-air charts upon which they are based, were composited in a different manner than the surface maps. Figure 3 shows a time cross-section relating the radiosonde observations to the composite period. The weighing ratios of 2:2:1 for the 1500 GMT December 21, 0300 GMT December 22, and 1500 GMT December 22 soundings respectively, were adopted.

III. KEYS TO THE WIND

SUMMARY

A combination of empirical and dynamic methods was employed to determine the three-dimensional wind flow. The greatest reliance was placed on empirical relationships (1) nearest the ground and (2) over the Central Valley (because of the more numerous observations there); the greatest use of dynamic methods was at higher elevations out of the reach of ground friction and over the mountains (because of the lack of observations there). An outline of the method for obtaining the wind is contained in table 1. In this list a "V/V_g" relation is an empirically-derived ratio of wind speed to geostrophic wind speed at a particular place and pressure (or elevation), or a similar relationship of wind direction to geostrophic wind direction. A schematic outline embracing the complete method, of which the wind is a part, is given in figure 4*a–c*.

GEOSTROPHIC SPEED RELATION

A series of comparisons was made between the wind speed and the geostrophic wind speed in order to detect the effect of friction on the wind. These were first reported in *Hydrometeorological Report No. 37* [7] (figs. 4–6 through 4–11). A summary of results is shown here. Figure 5 gives these V/V_g relationships. Curve "D" was used to determine input wind speeds for coastal range computations, while curve "C" was used for the Sierras.

690-385 O—63——2

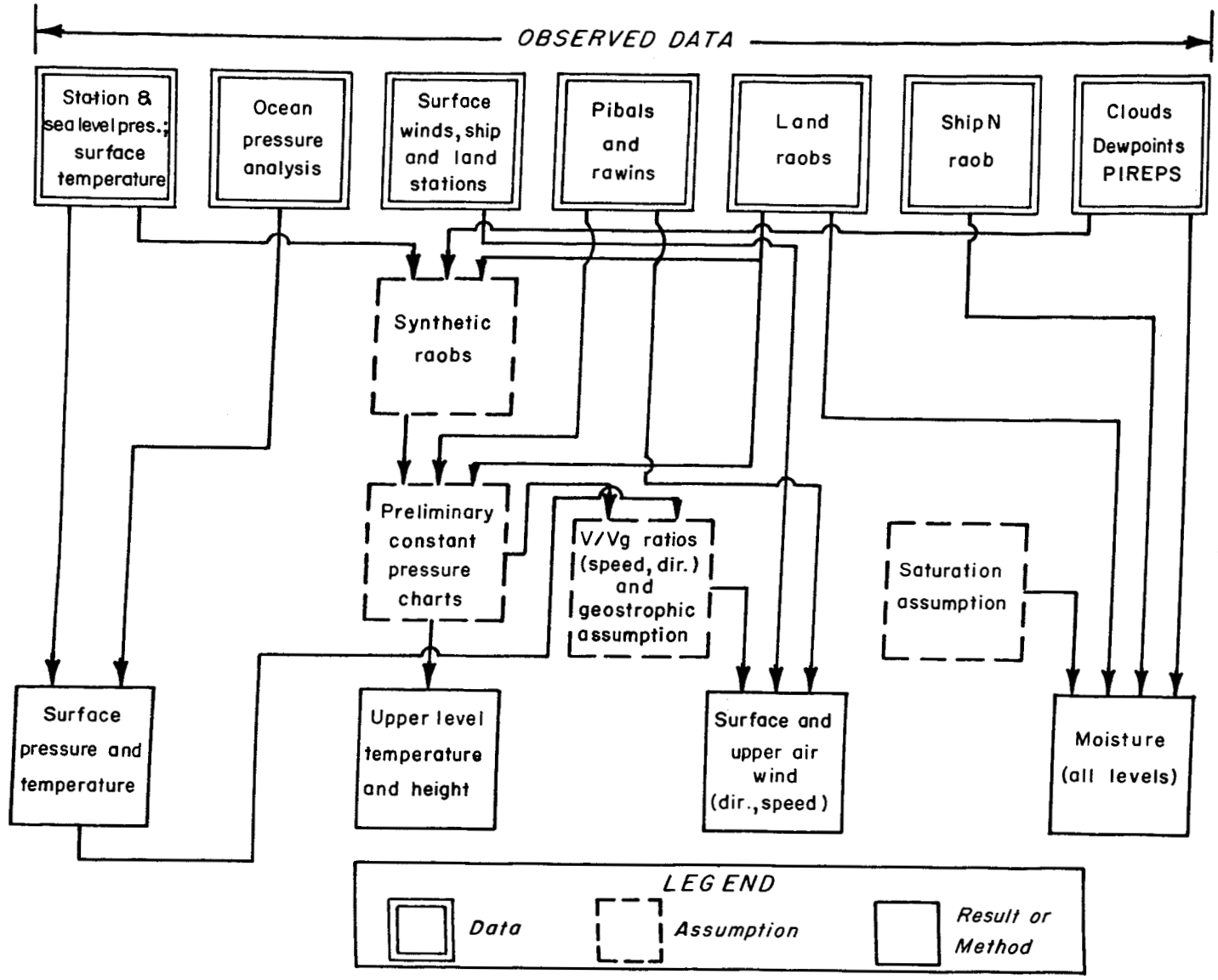

FIGURE 4.—Schematic diagram of the method of deriving the wind, temperature, and pressure at computation (outflow) points. (*a*) Basic data, observed and computed, for input into (*b*).

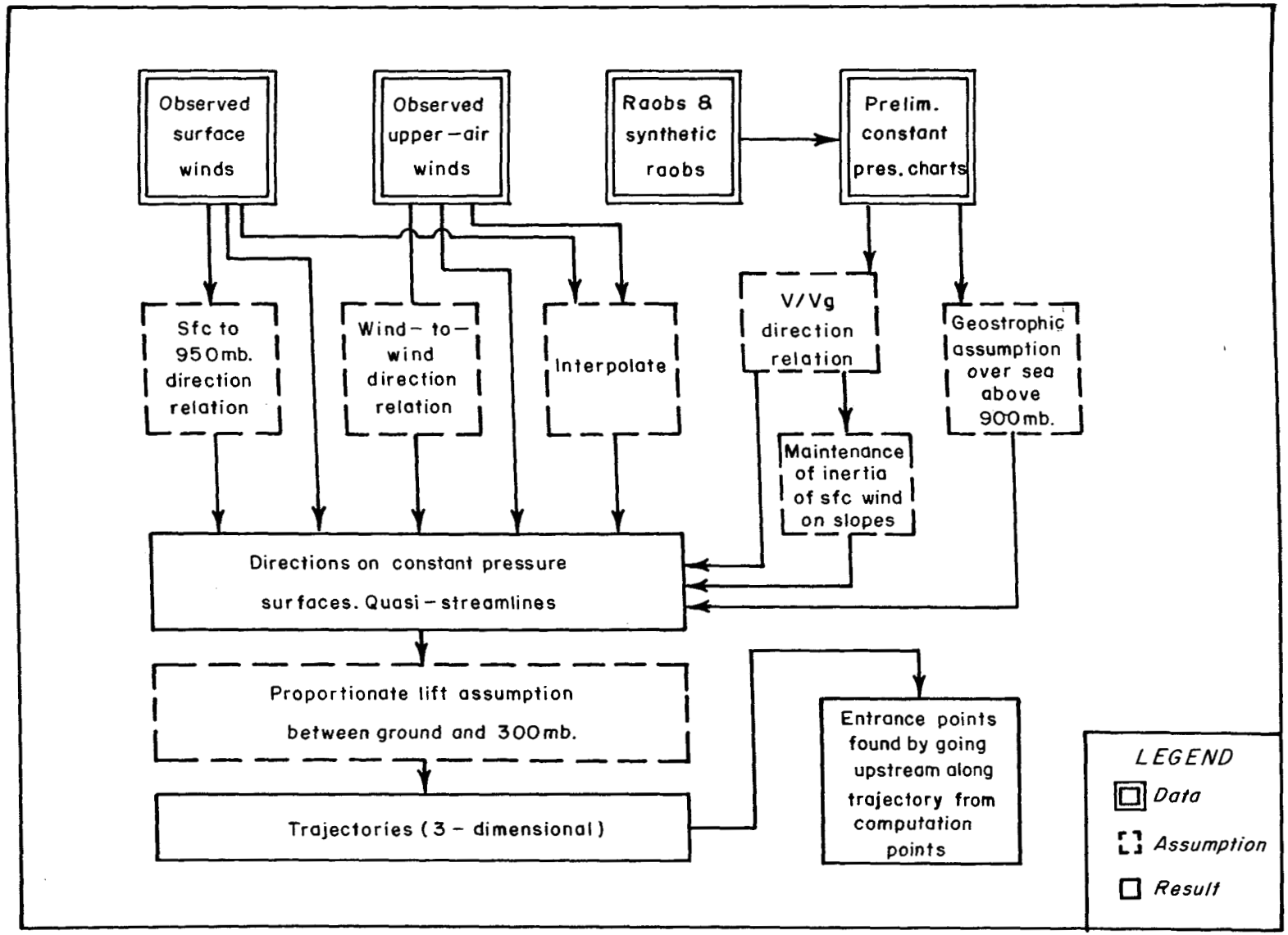

FIGURE 4.—(b) Procedure for obtaining first estimate of trajectories and of locating "entrance" points.

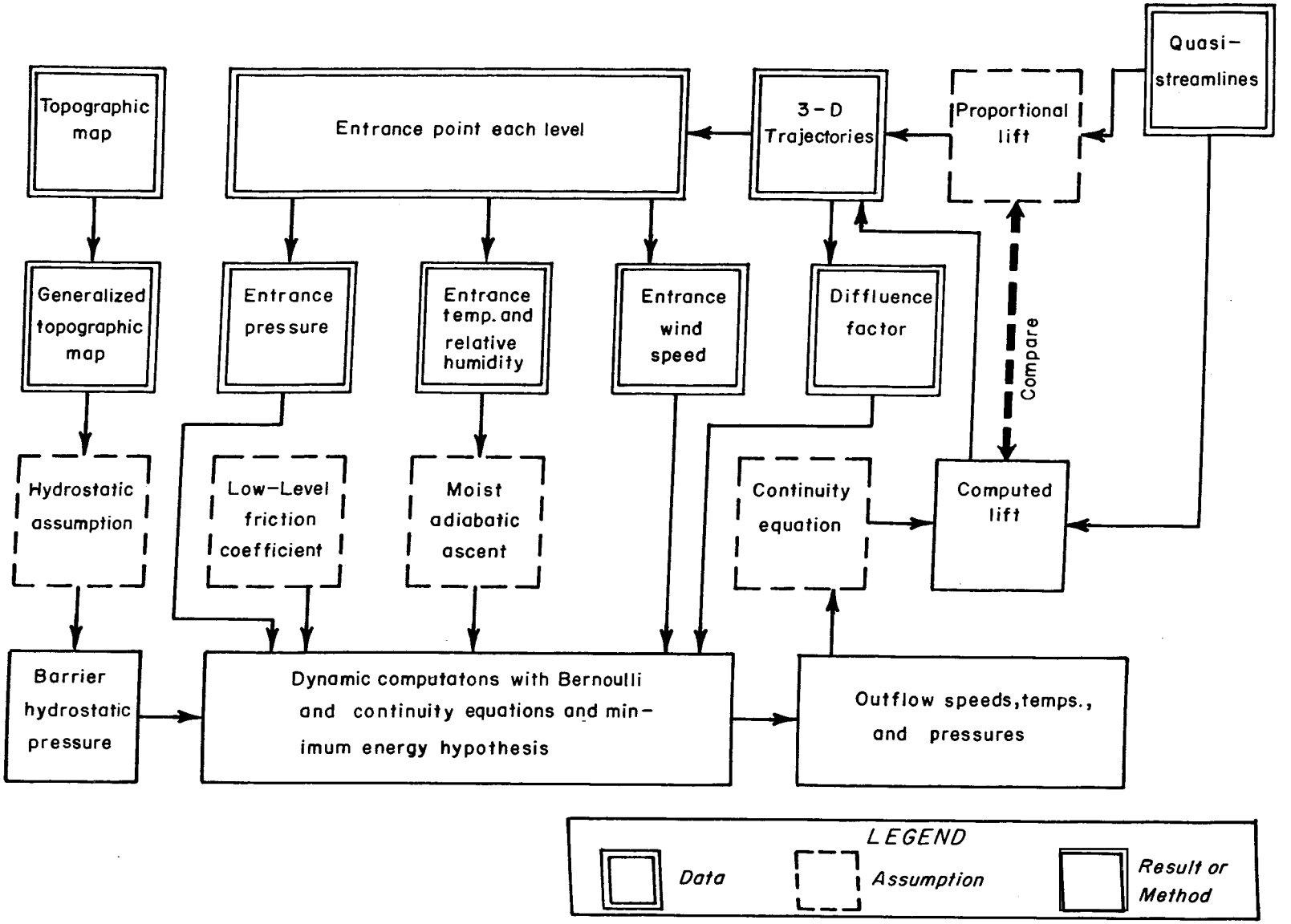

Figure 4.—(c) Steps in computing final wind speed, temperature and pressure for outflow points.

TABLE 1.—*Outline of procedures for reconstructing the wind*

1. OBSERVATIONS
   Composite wind observations were accepted where available, at surface and aloft
2. OVER THE SEA
   a. *900 mb. and above:* Geostrophic direction and speed.
   b. *Below 900 mb.:* V/V_g empirical relation, direction and speed.
3. OVER THE CENTRAL VALLEY
   a. *Speed, surface to about 900 mb.:* In order of decreasing influence: empirical relation to surface wind, V/V_g empirical speed relations, wind-to-wind relation, dynamic computation with friction.
   b. *Speed, 900 mb. to mountain crest elevation:* Intermediate between dynamic computation without friction and V/V_g empirical speed relation.
   c. *Speed, above mountain crest elevation:* Dynamic computation without friction.
   d. *Direction, surface to about 900 mb.:* Empirical relation to surface wind, primarily; V/V_g empirical direction relation secondarily.
   e. *Direction, 900 mb. to mountain crest elevation:* V/V_g empirical direction relation.
   f. *Direction, above mountain crest elevation:* Interpolated from observations and in accord with broadscale (but not local) geostrophic wind. This is a close approximation to a frictionless dynamic trajectory computation. Also conforms to V/V_g empirical direction relation.
4. OVER MOUNTAINS AND SLOPES
   a. *Direction:* Rapid turning of wind with height near surface. Persistence of coast and Central Valley direction along *3-dimensional* trajectory. At higher elevations same considerations as 3f.
   b. *Speed:* Dynamic computations with minimum energy hypothesis, from [2]. Surface friction layer of 100-mb. depth or less, frictionless above.

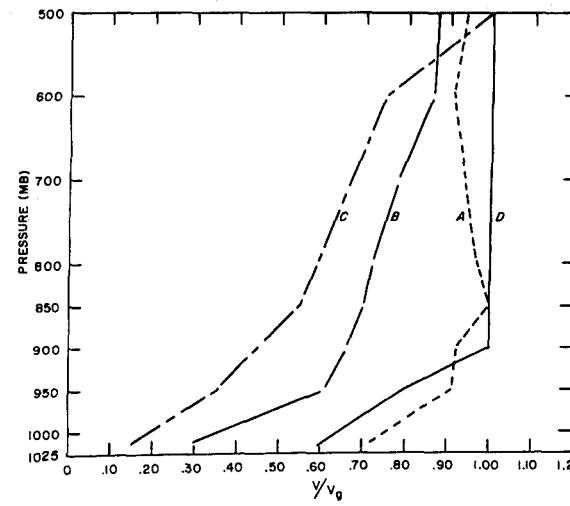

FIGURE 5.—Relation between wind speed V and geostrophic wind speed V_g for: (Curve A) over sea, uninfluenced by land; (Curve B) over land, but near coast; (Curve C) in the Central Valley; and (Curve D) over sea, but near land.

GEOSTROPHIC DIRECTION RELATION

The upper-air wind direction and its relation to the geostrophic wind direction was also investigated and presented in *Hydrometeorological Report No. 36* [6] (figs. 4–15, 4–16, and 4–17). The relationships were applied to the average geostrophic wind direction observed in the composite period to obtain an estimate of the actual wind over the areas and at the elevations indicated in the outline of table 1.

INCREASE OF WIND WITH HEIGHT

An empirical study was conducted to determine if a clear relation existed between the surface wind and the wind at 500 meters above sea level. The relatively large number of surface wind observations compared to upper-air wind observations makes the usefulness of such a relation apparent. Relationships were developed for several upper-wind reporting stations in California.

The mean curve for an individual station, Oakland, is shown in figure 5. (A sample plot of the surface–upper air relation for Oakland is given in figure 4–18 of [7], and the general relationship for obtaining an estimate of the 500-m. wind using surface wind and station elevation as arguments is presented in figure 4–19 of [7].)

TURNING OF WIND WITH HEIGHT

Turning of the wind with height was investigated for the same stations used in the speed study. Results of this study (not shown) indicate that, on the average, storm winds veer from the surface to 500 m. at all stations, with less turning of wind in the Central Valley than at coastal locations.

TENTATIVE TRAJECTORIES

Tentative three-dimensional trajectories were developed throughout the volume of study, except at lower levels over the Central Valley, by the following steps.

1. *Quasi-streamlines* were constructed on selected constant pressure surfaces by the techniques listed in table 1. A quasi-streamline in this report is a curve drawn on a constant pressure surface in the usual manner of streamlines, connecting the components of the three-dimensional wind direction along that surface. An example, the 800-mb. quasi-streamlines, is shown in figure 6. A *streamline* or *trajectory* is understood to be three-dimensional in this report.

2. Trajectories at the ground follow the ground slope. This inclination to the horizontal of trajectories was assumed to diminish linearly on a pressure scale to horizontal flow at 300 mb.

3. Directions of flow from the quasi-streamlines were interconnected into three-dimensional trajectories with assumption 2. It was found that tra-

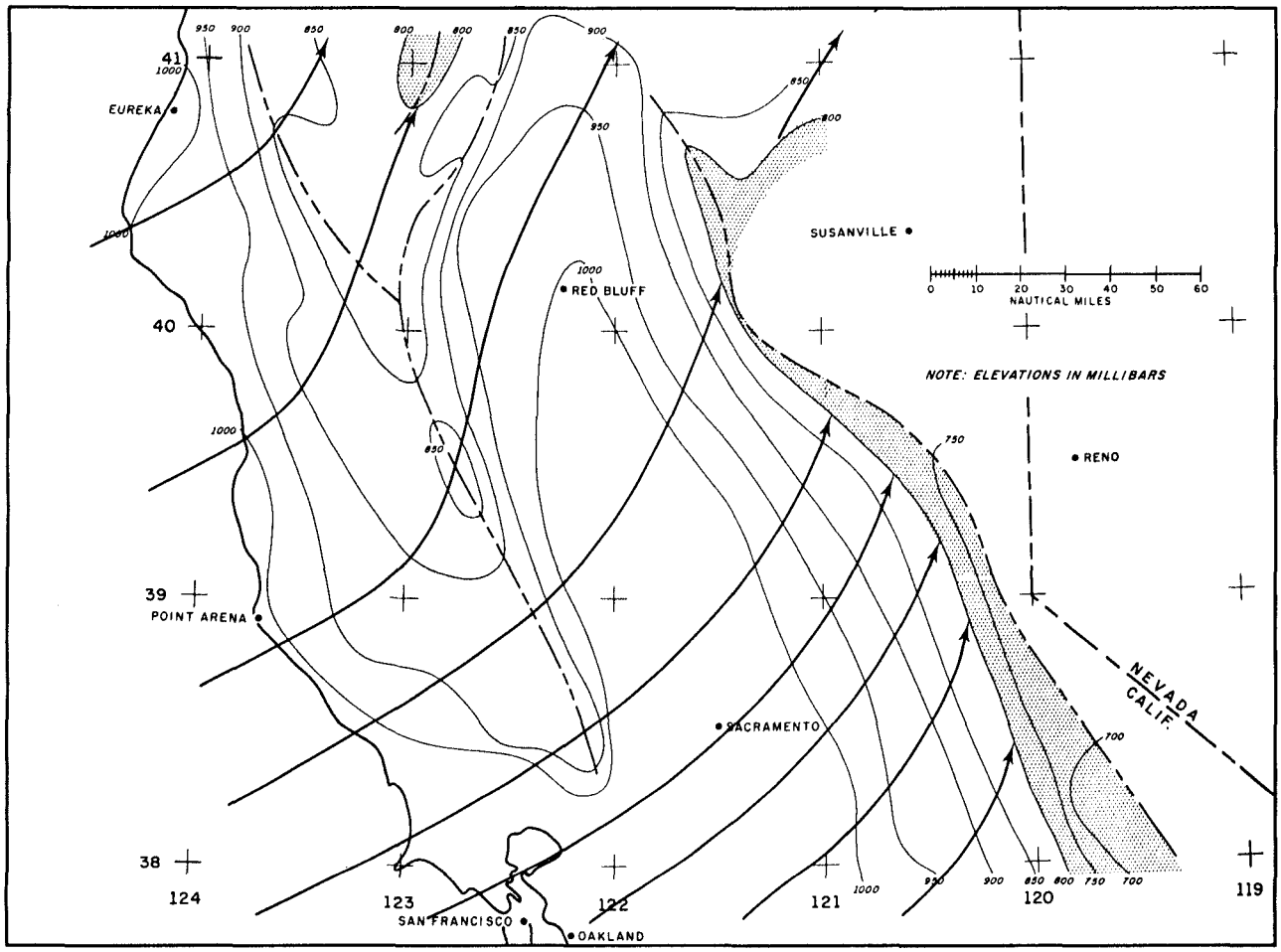

FIGURE 6.—Example of a quasi-streamline chart (for 800 mb.) used in constructing three-dimensional trajectories. Shading cuts off area of topography higher than 800 mb.

jectories showed much less curvature than quasi-streamlines. Figure 7 gives the trajectory construction for a coast range computation point.

DYNAMIC TRAJECTORIES

A trajectory is a curve tracing the path occupied by a particle in motion. A "dynamic" trajectory is one in which the particle path is computed by the equations of motion from values of the forces acting on the particle. The following conditions must be met, however, if realistic results are to be obtained: (a) frictional influences must be small (or must be taken care of by frictional coefficients); (b) speed and direction of the air must be known or closely approximated at the initial or some other point on the trajectory; (c) changes in the pressure gradient as the parcel moves from one level to another should be allowed for.

As a test, some dynamic trajectories were computed on the preliminary version of constant pressure charts to compare with the tentative trajectories computed by the graphical method outlined above. It was found that the two methods yielded similar results. An example, one for 700-mb. inflow, is shown in figure 8. Here the maximum difference in wind direction is about 12°.

These test dynamic trajectories showed, at higher levels above frictional effects, that air parcels traverse the storm study area with significant fluctuations in speed but with only slight change in direction. This results, in part, from

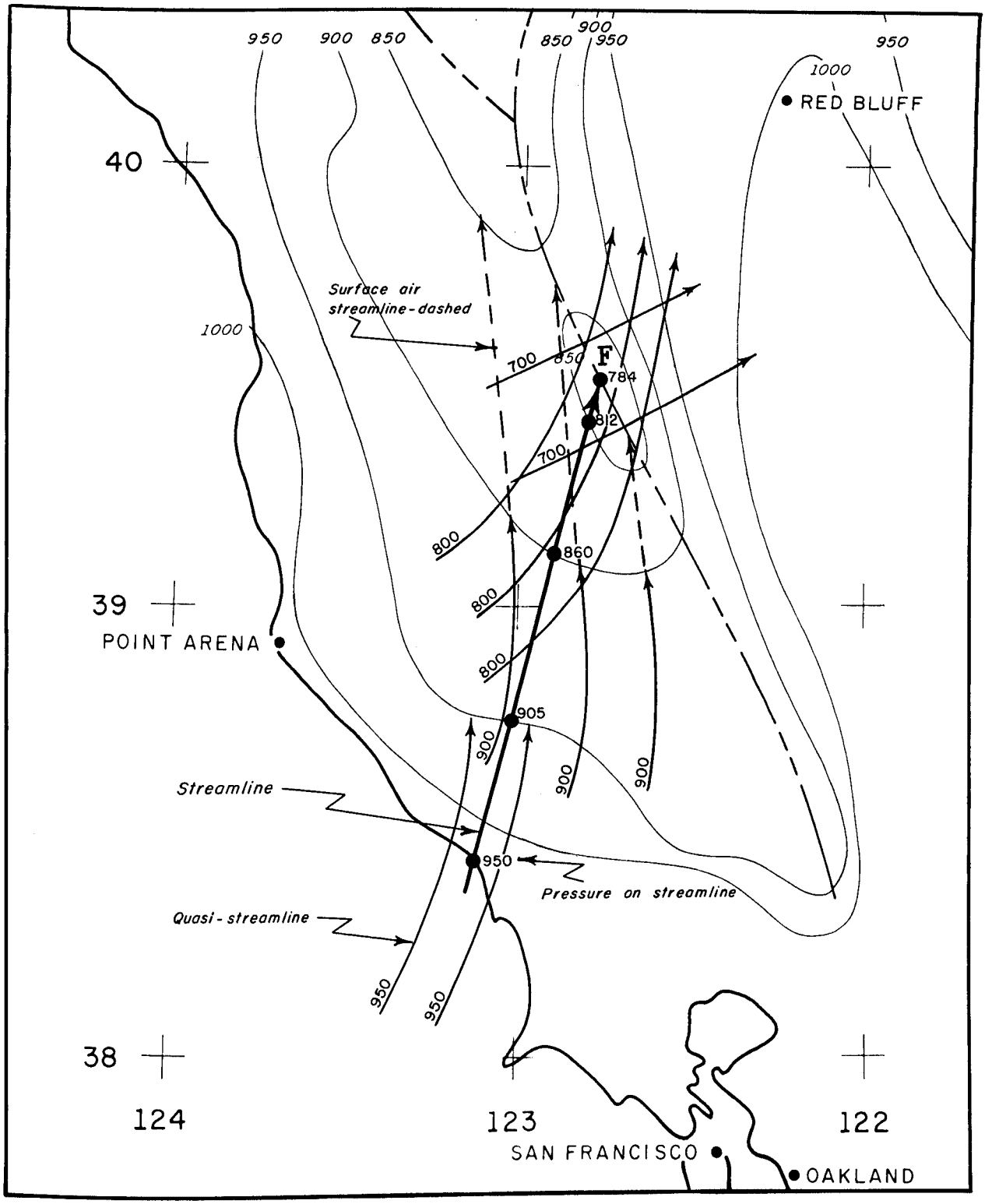

FIGURE 7.—Example of trajectory construction by the graphical method from the quasi-streamlines for a computation point (F) in the Coast Range.

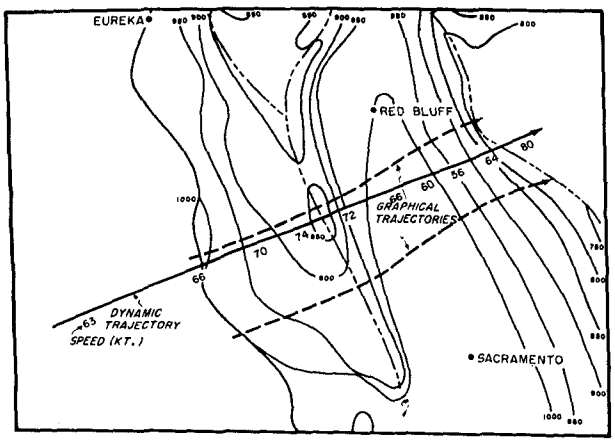

FIGURE 8.—Comparison of trajectories constructed by graphical method (as in fig. 7) with "dynamic" trajectories computed from the equations of motion. This one is for 700-mb. inflow.

the pressure gradient distribution; the component normal to the flow does not change much while the component along the flow is subject to large variation, even reversing its direction. It is probably valid to generalize that such a marked change in speed with only a slight change in direction is characteristic of flow in depth over a long continuous ridge.

Thus it was possible to construct a dynamically consistent model by a combination of rigorous dynamic computation of speed along trajectories and reliance on less laborious empirical methods to lay out the directions of the trajectories.

THE MINIMUM-ENERGY METHOD OF COMPUTING SPEEDS OVER A RIDGE

A method of computing the two-dimensional wind flow over a ridge from a given inflow at the foot of the ridge has been previously cited [2]. A brief summary of this method is given in section VII of this report. The method, in effect, uses the Bernoulli equation along a streamline to compute the speed change along the streamline, adiabatic laws to determine the variation of temperature along a streamline, and the continuity equation and the hydrostatic equation to give the spacing between streamlines. A minimum-energy analogy to water flow is then used to select the outflow over the ridge crest from the family of such outflows that fit the combination of equations cited.

This two-dimensional method is carried forward into the present study and is applied along sets of tentative trajectories. In this application a point is selected on a ridge crest (or other point) as an outflow computation point. Tentative three-dimensional trajectories that terminate at various elevations above this point are then constructed. The inflow pressure, temperature, and wind speed at the coast (or at the southern edge of the study area) at the beginning point of each of these trajectories then becomes the inflow data for an electronic computer determination of the outflow at the selected computation point. In the original two-dimensional method of [2] all the inflow points are in a vertical column. In the application here they are not. This is taken care of by introducing a factor to be explained in the next section.

The two-dimensional study [2] includes an allowance for friction in a surface layer of variable thickness. This method is carried forward into the present study with some changes in the friction coefficients, based on comparison of computed and observed surface pressures at check points such as Red Bluff and Blue Canyon.

The computation yields a wind speed, pressure, and temperature for each trajectory at the outflow computation point. These computed pressures are compared with the pressures on the tentative trajectories and second approximations carried through where required.

THE CENTRAL VALLEY TECHNIQUE

At lower levels in the Central Valley, air streams northward, essentially parallel to the ridges. Where and how much the air climbs the ridges as the valley narrows, or whether the air passes through the lesser space by speeding up, is not known a priori. The proportional lift to 300 mb. was considered dubious for the tentative trajectories. Here direct use was made of the trajectories themselves, starting at the surface, to determine the lift. The air parcels were followed by means of a mesoscale cross-sectional analysis to be described in section VI.

IV. SURFACE WIND AND PRESSURE

SEA LEVEL PRESSURE

The basic sea level pressure chart, to which all upper-air charts were fitted, is shown in figure 9. The chart includes all surface observations, which are mostly at lower elevations, and the theoretically derived sea level pressures for the higher elevation analysis. The manner of deriving the latter is described later.

The sea level analysis reveals a strong geostrophic wind vector from about 240° over the adjacent Pacific Ocean. Strongest winds are concentrated near 40° N., while the winds are weaker south of 38° N. and also slightly weaker north of about 41° N. A very slight trough in the isobars is evident near Cape Mendocino, about 40°30′ N., 124°30′ W. It was not determined whether this trough was induced by the coastal configuration or was due to a slight instrumental error at the Blunts Reef Lightship (the station immediately offshore of the Cape). A well-marked trough generally 2 to 3 mb. deep is centered along the Coast Range ridge line. At the break in the coastal range near San Francisco, the coastal range trough is much weaker, barely 0.5 mb. deep.

In the Central Valley, pressure recovers completely from the coastal trough. If the sea isobars are projected inland to the Central Valley the pressure returns to "normal" a few miles east of the valley center. A pressure "excess" of perhaps 1 to 2 mb. follows on the Sierra Nevada upslope centered about half-way to the crest. To the east of the Sierra crest, at a distance of about 50 n. mi., lies a very pronounced trough 5 to 6 mb. deep. The position of this trough with respect to its parent mountain range is unlike the coastal trough position which is centered very near the ridge line itself.

SURFACE WINDS

The mean wind flow at the earth's surface (anemometer level) for the composite period is depicted by the streamlines on figure 10, drawn to the vector mean winds for the individual stations.

The surface wind flow in the Central Valley and along the coast is well defined, but the flow on the higher mountain slopes and ridges is more speculative due to the smaller number of observations. Blue Canyon (on the Sierra Nevada) at 5300 ft., Mt. Hamilton, 4200 ft., and Sexton Summit, 3800 ft., are virtually the only direct sources of information in these critical areas. Observations at these stations indicate that there is a marked difference between the surface wind direction at an upper elevation and the free-air wind direction at the same level nearby. Mount Hamilton is situated roughly between Merced and Oakland (fig. 2), about 50 n. mi. from the former and 30 n. mi. from Oakland. The composite surface wind at

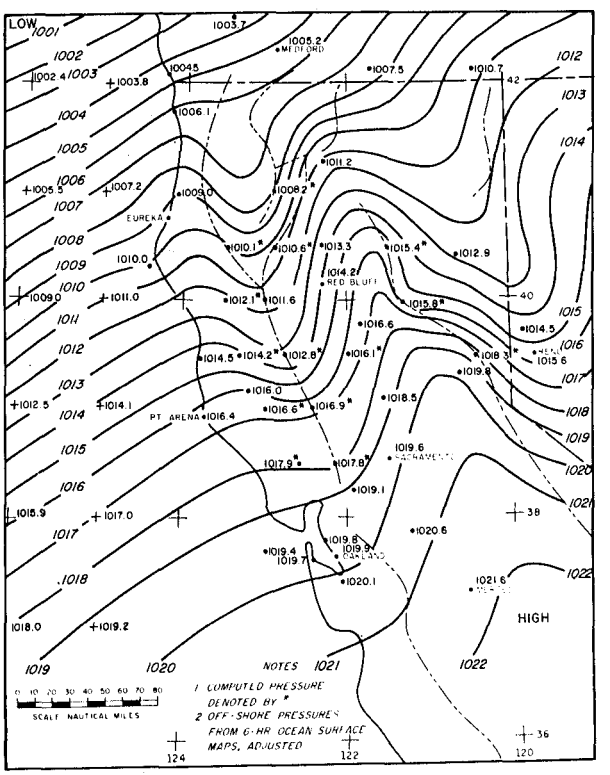

FIGURE 9.—Mean sea level pressure chart based on hourly observations for period 0400 PST December 21 to 0400 PST December 22, 1955.

690-385 O—63——8

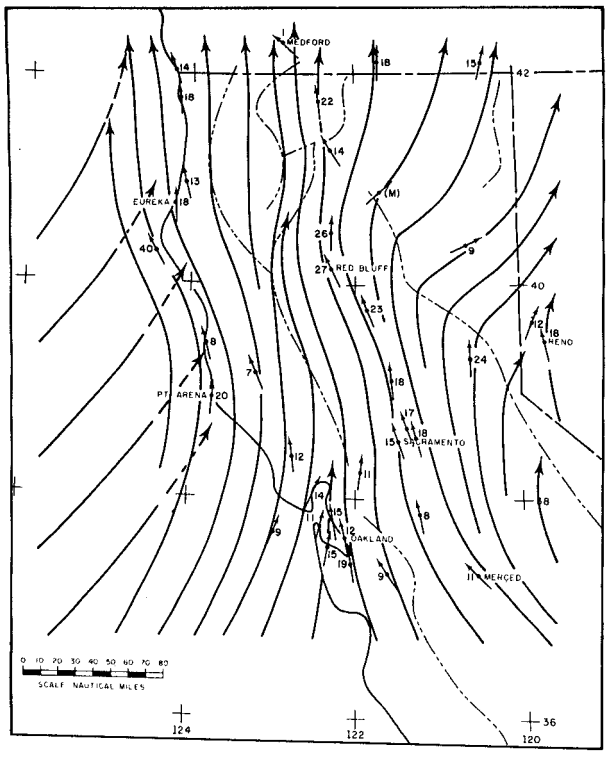

FIGURE 10.—Composite surface streamline chart. Speeds in knots.

Mt. Hamilton differed by 60° from the free-air wind direction as estimated from the rawin observations (fig. 11) but was about the same as nearby low-level surface flow. (The mean direction at Mt. Hamilton was 147°, while at San Jose, at the foot of the mountain, it was 149°.) Similarly, Marysville in the Central Valley reported a wind direction of 173° while Blue Canyon, far up the slope, reported 177°. Farther north at Sexton Summit, the mean wind direction was 173°. No observing station is available at the foot of this mountain for comparison purposes; however the valley to windward is oriented in a north-south direction, making it probable that a southerly wind was blowing there.

On the basis of these cases and a few wind directions reported by cooperative observers it is surmised that the surface airflow on the windward face of the coastal and Sierra slopes up to the crest had a direction very close to that in the Valley below, i.e., parallel to the generalized ground elevation contours. It follows that a

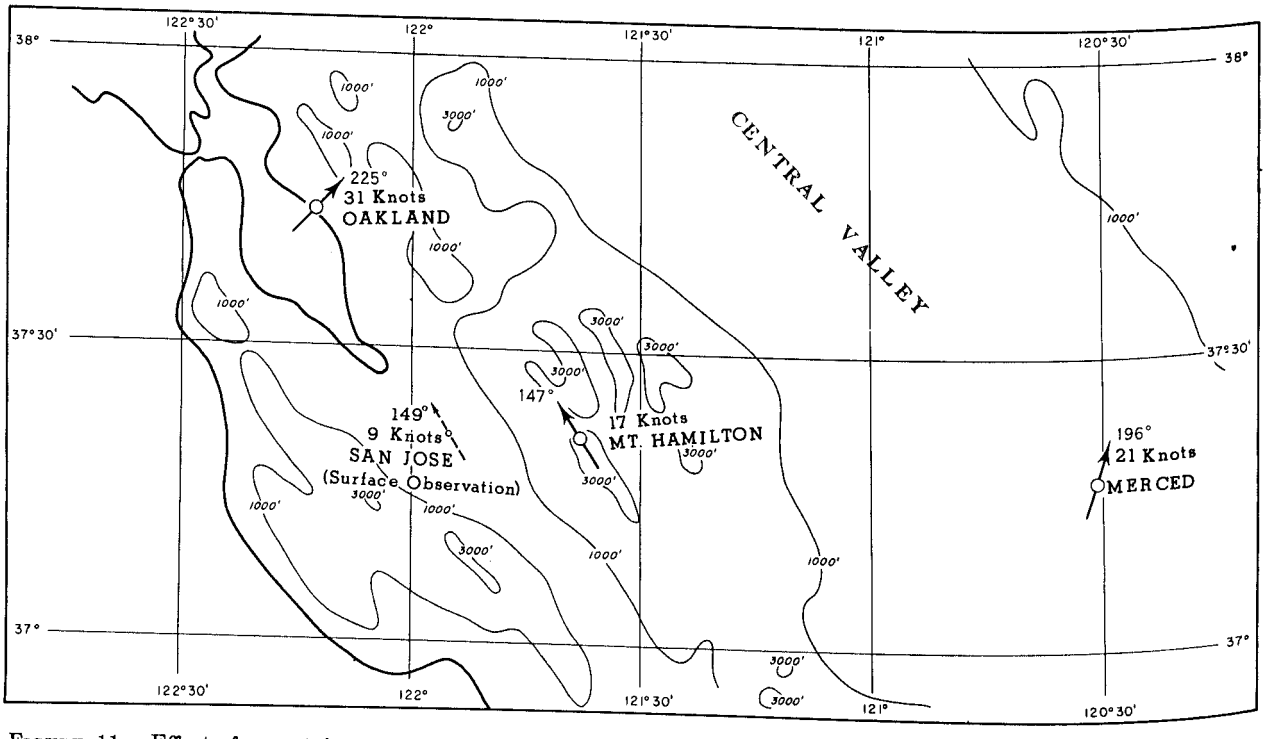

FIGURE 11.—Effect of mountains on free-air wind. Wind at Mt. Hamilton is observed surface wind. Winds at Merced and Oakland are from the rawin at the 860-mb. level (the height of Mt. Hamilton). San Jose's wind is a surface observation at a low-elevation station.

pronounced wind shear must exist immediately above a ridge or slope, especially at higher slope elevations.

For wind analysis over the ocean, ship observations provided the only direct source of data but were not suitable for compositing. Individual ship reports did indicate, nevertheless, a basic current from between south-southwest and southwest for the composite period at about 100 mi. off the coast. This current, as it approached the northern California coast encountered a coastal current from a southerly quarter, and is assumed to have ridden up over it since the open ocean wind current had the higher temperature. The composite wind direction at Blunt's Reef Lightship in the coastal current was 40 kt. from 150° (see fig. 10). Dynamic trajectory analysis, taking the prevailing pressure field into account, suggests that it would have been impossible for the air current from the open ocean to make such a rapid turn in direction (from 215° to 150°) in a few hours time at such a high speed. The dashed part of the trajectories shows the assumed area of lifting of the air current from the southwest.

V. SYNTHETIC TEMPERATURE SOUNDINGS

Because of the wide spacing of upper-air soundings, the Oakland, Merced, and Medford raobs were used as guides to construct a number of hypothetical or synthetic temperature soundings. Locations of synthetic soundings are given in figure 24.

The synthetic soundings integrate all available data that could possibly be used as clues to upper-air conditions. Items taken into consideration in construction of the soundings include: (a) station pressure, temperature, and humidity; (b) general weather conditions at the station with special reference to clouds and precipitation; (c) interpolated upper-air temperatures and humidities between raob stations; (d) aircraft weather reports in the vicinity of the station (usually consisting of height of cloud tops and bottoms, icing, and precipitation observations); (e) nearby mountain temperature at same level.

Figure 12 shows a sample composite synthetic sounding to 300 mb. for Point Arena, Calif. The surface temperature, pressure, and relative humidity were taken from composited surface readings. The saturation point at 960 mb. was obtained from the mean observed cloud height. Temperatures and humidities aloft were derived mainly by interpolation between raobs. Aircraft and Ship N reports also assisted.

All of the soundings, synthetic and actual, were used in construction of the first approximation constant pressure charts. The three coastal synthetic soundings together with the Oakland raob were the primary basis of the inflow temperatures and pressures used for dynamic computation of flow over the Coast Range, and of moisture for the subsequent computation of precipitation. The Red Bluff and Sacramento synthetic soundings and a computed sounding at 39°30′ N., 122° W., together with the Merced raob performed a similar function for Sierra computations. The soundings at Red Bluff and at 39°30′ N., 122° W. were used as terminal points on downslope computations from the coastal range to check preliminary temperatures. A few slight adjustments were required.

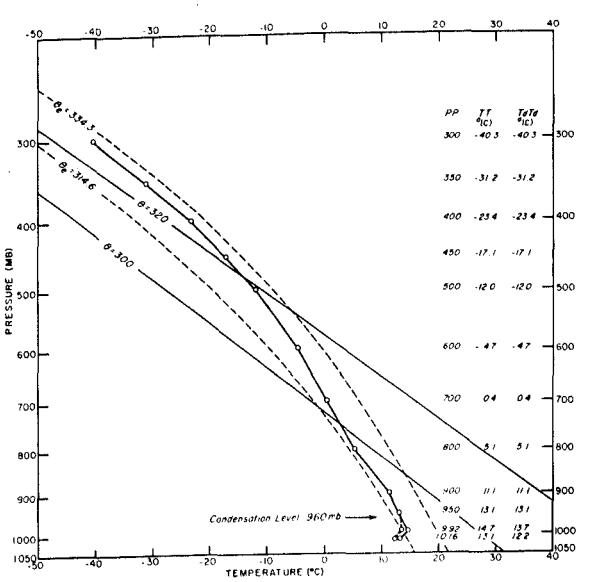

FIGURE 12.—Composite synthetic temperature sounding for Point Arena.

VI. CONFINED FLOW IN THE CENTRAL VALLEY

CENTRAL VALLEY PROBLEM

The low-level air current over the Central Valley presents a special problem. The confined flow, channeled between the Coast and Sierra Ranges must contend with a Pacific air current coming over the coastal ridge for the air space over the Valley. This is especially true at the northern end of the valley where the ground itself rises sharply. In consequence, the amount of descent, if any, of the ocean air currents must be determined. The method chosen for this study was cross-sectional analysis.

CENTRAL VALLEY CROSS SECTIONS

Five east-west cross sections of horizontal component of wind direction and wind speed were constructed to study the Valley flow in detail. These were made for 30′ intervals from 38°30′ to 40° N. from Coast Range to Sierra ridge lines. A sample, that for 38°30′ N., is shown in figure 13. The wind directions are from the quasi-streamline maps while the speeds over the low ground are estimated by the various aids discussed in section III. Over the coastal ridges the total wind speeds were derived from results of preliminary application of the theory to be discussed in section VII.

Tracing of the motion of a parcel from one section to another in three dimensions was completed by application of the continuity equation to the wind field. Figure 14 shows a sample analysis, that from the cross section

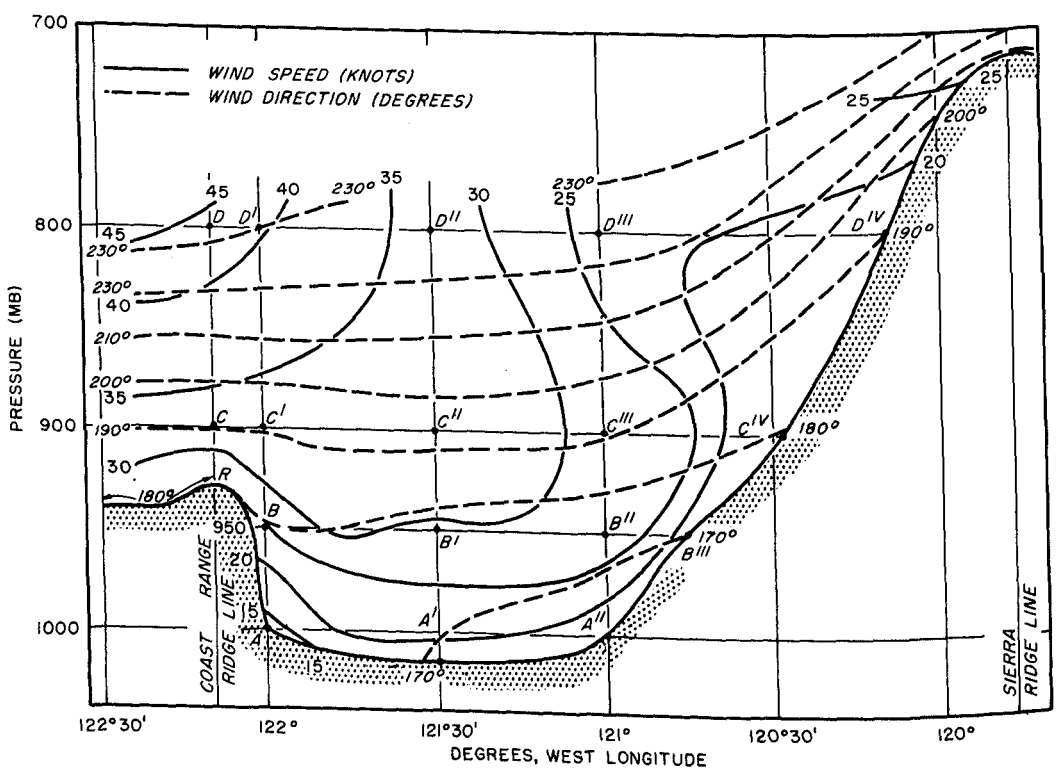

FIGURE 13.—Section across the Central Valley at 38°30′N., showing horizontal components of wind direction and speed. Wind directions are from the quasi-streamline maps and speeds are estimated by the methods described in text. Points labeled with letters are carried forward into figure 14.

38°30′ to 39°. The rectangular grid pattern shown at 38°30′ is distorted by the winds to the slanted grid pattern at the 39° cross section. The hatched pattern represents new air that has come in over the Coast Range ridge line between the two cross sections. The open grid box over the Sierra crest at the right of the diagram indicates some air has escaped the Central Valley between these two cross sections. As illustrative of the method used to obtain the 39° positions, consider the segment A–B. On the 38°30′ cross section A marks the ground position at 122° W. and B the 950-mb. 122° W. intersection. Point A on the 39° cross section is derived from the surface trajectories. It is asumed that surface air remains on the surface. The point B on the 39° cross section is located by (1) moving the 38°30′ point B along the 950-mb. quasi-streamline (this position is marked by $\overline{B}$) and (2) obtaining a corrected (in pressure) position (B) by the continuity formula $\Delta p_2\overline{V}_2=\Delta p_1\overline{V}_1$ where subscript 2 refers to the 39° section and subscript 1 to the 38°30′ or initial cross section. In this case no direction correction was necessary, since the 950-mb. wind direction and the 960-mb. wind direction are virtually the same. In a few cases where the pressure-corrected position had a significantly different wind direction a second approximation was made. The continuity formula used is valid where the quasi-streamlines at any one level are virtually parallel. The 950-mb. and 900-mb. quasi-streamlines over the Central Valley (not shown) meet that requirement.

The above streamline analysis was carried from section to section until the streamline disappeared either over the Sierras of out through the northern end of the Central Valley. (A few very low-level streamlines crossed the Coast Range ridge line.) Enough streamlines were traced through the cross sections to show the probable path of the ocean air entering the Central Valley airspace from between the Coast Range ridge line and 800 mb.

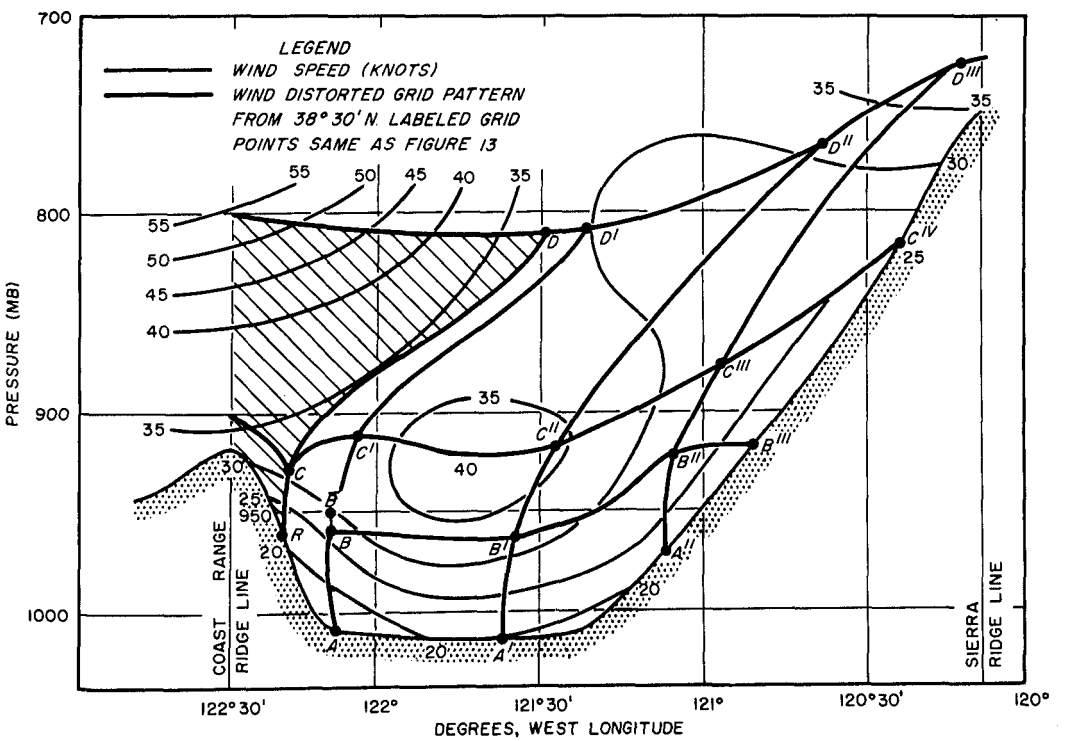

FIGURE 14.—Section across the Central Valley at 39°N., showing distortion of the labeled grid pattern of figure 13 by the wind. See text for explanation. Hatched area represents "new" air which has entered valley over Coast Range crest.

RESULTS OF CROSS-SECTIONAL ANALYSIS

There seems to be little doubt that the air both speeds up and climbs the face of the Sierras as it flows northward through the narrowing Central Valley. The axis of maximum speed shows increases from about 35 kt. at 38°30′ to 55 kt. at 40°30′. Analysis reveals that this low-level wind maximum was located near the center of the valley at an elevation of about 3000 ft. The speed-up is reflected in the surface wind speed observations, which increase from 15 kt. at Sacramento to 27 kt. at Red Bluff (see fig. 10). The cross sections reveal that a substantial volume of valley air escapes over the Sierras. Wind observations just to the east of the Sierras (e.g., Burney and Susanville) confirm this. The bulk of the low-level air, however, is forced to make an abrupt ascent at the northern end of the valley between Mt. Shasta and Mt. Lassen.

The analysis on the eastern slope of the Coast Range is more doubtful because of the lack of observations. The best estimate is that some of the low-level air in the extreme northern Central Valley escapes over the Coast Range ridge line. In the more southerly portion (south of about 40° N.), the low-level air has a downslope component except in very restricted areas. All air above the 850-mb. level probably crosses the Coast Range divide from west to east. Air crossing the ridge into the Central Valley (except air on the surface), does not descend as much as the ground level does. For example, air on the 39° cross section (fig. 14) that enters at 800 mb. descends only about 10 mb. to the center of the Central Valley, while the ground itself drops away about 95 mb. in the same distance. This situation of almost level flow at 800 mb. from ridge to valley prevails up to the northern reaches of the Central Valley. At the northern exit from the Valley, the air probably rises at all levels. That is, the combination of rising ground and the remaining volume of the valley current necessitate a continued climb of the ocean air from coastal ridge to valley center.

Partial verification of the derived Central Valley analysis was obtained from the dynamical computation of the wind to be described in the following section (VII). In the numerical computations the speeds and pressures are calculated, but the direction (or horizontal projection of the path) is not directly verifiable by this method. Numerical computations confirmed the speeds and pressures used along the preliminary trajectories.

VII. DYNAMIC COMPUTATION OF WIND SPEED

Several changes were made in the mathematical basis for computation of two-dimensional wind flow given in [2] for application to three-dimensional flow. First, it is apropos to review the steps in the two-dimensional method.

TWO-DIMENSIONAL WIND FLOW

The vertical wind profile above a ridge crest point is obtained from the inflow variables at the foot of the ridge by the following steps. Subscripts pertain to the points shown in figure 15*a*.

1. A tentative surface wind speed, V_2, is assigned at the ridge crest.

2. The ridge crest surface pressure, p_2, necessary to produce V_2 with a designated friction coefficient, k_1, is computed from the inflow variables and the hydrostatic pressure at the ridge crest, $(p_2)_h$, by equation (18) of [2] (repeated as equation (11) in this paper) and the adiabatic laws of temperature variation.

3. The outflow pressure, temperature, and speed, p_4, T_4, and V_4, on a second streamline vertically above the first one are computed from the inflow variables and the surface variables by simultaneous solution of the laws of adiabatic temperature variation, the energy equation,

$$\frac{1}{k_3}(V_4^2-V_3^2)-\frac{1}{k_1}(V_2^2-V_1^2)=2RA, \qquad (1)$$

and the equation of continuity

$$(V_1+V_3)(p_1-p_3)=(V_2+V_4)(p_2-p_4) \qquad (2)$$

These are equations (15) and (10) in [2]. A is defined below and R is the gas constant for air.

4. The outflow variables on another streamline, proceeding upward, are determined by repetition of step 3, working from the streamline just computed.

5. The process is continued stepwise upward beyond the first nodal surface (where $p_3=p_4$).

6. The computation is repeated with a succession of different tentative surface outflow speeds, V_2.

7. The computed profile is selected which has the least value of $(V_4^2-V_3^2)$ at the first nodal surface. The logical basis for this selection is explained in section 5 of [2].

8. Outflow computations for the selected profile are continued upward from the nodal surface to the desired height or until the computations fail ([2] p. 4276).

In the above development A is defined by

$$A=-\oint Td(\ln p) \tag{3}$$

and is approximated by

$$A=\tfrac{1}{2}[(T_1+T_3)\ln(p_1/p_3)+(T_3+T_4)\ln(p_3/p_4) -(T_1+T_2)\ln(p_1/p_2)-(T_2+T_4)\ln(p_2/p_4)] \tag{4}$$

for machine computations.

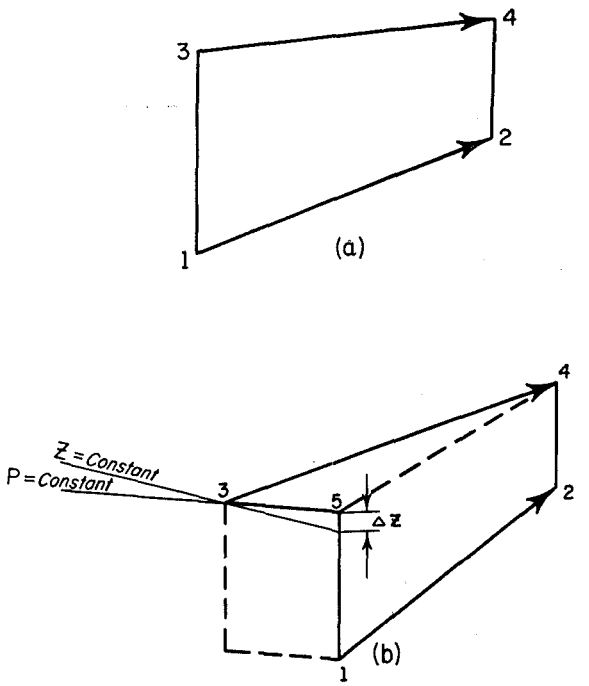

FIGURE 15.—(*a*) Diagram for two-dimensional wind flow computation. (*b*) Modifications to (*a*) for three-dimensional computation.

CHANGES IN METHOD FOR THREE-DIMENSIONAL FLOW

The non-vertical adjustment. The first adjustment to the two-dimensional method takes account of the fact that the trajectories along which speeds are computed are not contained in a vertical plane. Speed variations were calculated along sets of trajectories which terminated at the same vertical but with initial points on different verticals, as illustrated in figure 15*b* for one pair of such trajectories. In this diagram the inflow point 3 and the point 5, vertically above 1, lie on the same pressure surface. The most essential difference from the two-dimensional computation is that the potential energy represented by $g\Delta Z$, where $\Delta Z=Z_5-Z_3$, is not available to accelerate the air and is subtracted from the right-hand side of equation (1). A factor of 2 appears because the left-hand side of equation (1) is double the kinetic energy variation.

A second adjustment is a computational convenience. The first product within the brackets of equation (4) is an integration of equation (3) in the vertical and now becomes $(T_1+T_5)\ln(p_1/p_5)$. Recalling that $p_3=p_5$ and letting $\Delta T=T_5-T_3$ the product is converted

$$(T_1+T_5)\ln(p_1/p_5) =(T_1+T_3)\ln(p_1/p_3)+\Delta T\ln(p_1/p_3) \tag{5}$$

For a computation equation, the definition of A is left in the form of equation (4). This A includes the first term on the right of equation (5). The second term on the right of equation 5 is applied as a correction. We now have as the energy equation for the three-dimensional flow, applying the two corrections to equation (1),

$$\frac{1}{k_3}(V_4^2-V_3^2)-\frac{1}{k_1}(V_2^2-V_1^2)=2RA+F \tag{6}$$

where

$$F=R\Delta T\ln(p_1/p_3)-2g\Delta Z \tag{7}$$

F is evaluated for each trajectory from the p_3 constant pressure chart and is part of the inflow data.

Confluence adjustment. The third adjustment for the three-dimensional flow is to the equation of continuity. The projections of horizontally adjacent trajectories on constant pressure surfaces are not necessarily parallel. This lack of parallelism is trivial in some parts of the flow but quite appreciable in others. The equation of continuity becomes

$$(D_1+D_3)(p_1-p_3)(V_1+V_3) = (D_2+D_4)(p_2-p_4)(V_2+V_4) \quad (8)$$

The D's are the distances between adjacent trajectories in the vicinity of the respective points 1, 2, 3, 4 of figure 15*b*. D_1 and D_3 were assigned arbitrary values of 15 to 40 nautical miles and the resulting D_2 and D_4 were scaled from charts of tentative trajectories.

For computation, a confluence factor C was defined as

$$C=\frac{D_2+D_4}{D_1+D_3}\approx\frac{1}{2}\left[\frac{D_2}{D_1}+\frac{D_4}{D_3}\right] \quad (9)$$

and the equation of continuity became

$$(p_1-p_3)(V_1+V_3)=C(p_2-p_4)(V_2+V_4) \quad (10)$$

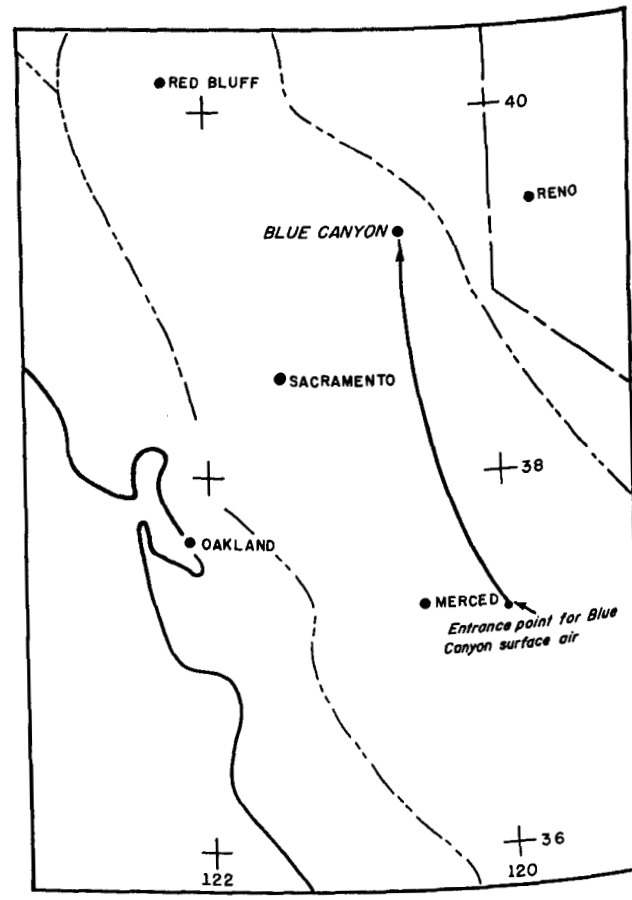

FIGURE 16.—Surface trajectory for air terminating at Blue Canyon.

OTHER ELEMENTS IN DYNAMIC COMPUTATIONS

Friction coefficient and observed surface pressure. Termination of a trajectory at a weather station gives an opportunity to compute the friction coefficient, k_1, and also qualitatively to verify some aspects of the method. Consider for example the surface trajectory shown in figure 16 terminating at Blue Canyon. The initial speed on this trajectory, V_1, is estimated at 16 kt. while the observed composite speed at Blue Canyon, V_2, is 23.7 kt. The "hydrostatic" surface pressure at Blue Canyon, $(p_2)_h$, is 843.5 mb. while the actual observed composite surface pressure, p_2, is 841.2 mb. The interrelation of surface speeds, pressures, and friction coefficient is given by equation (18) of [2,] repeated below

$$R\overline{T}_{1-2}\ln\frac{p_2}{(p_2)_h}+\frac{1}{2k_1}(V_2^2-V_1^2)=0 \quad (11)$$

The explanation and derivation of the equation are contained in the original paper. $\overline{T}_{1-2}$ in this instance is 282.7° A. Inserting all the other variables and solving for k_1 yields a value of 0.27.

However the flow must also fulfill the condition that it is the minimum energy outflow. That is, for a given friction coefficient, what outflow speed V_2 and outflow pressure p_2 yield outflow profiles extending from the ground into the stratosphere which fulfill the minimum energy condition? Trials were made with various k_1's; it was found that for the Blue Canyon case a k_1 of 0.25 would yield the correct outflow surface pressure p_2. This k_1 was adopted for that portion of the Sierra Nevada. The computed outflow surface speed for this k_1 is 22.0 kt. instead of the observed 23.7. Smaller k_1's (more friction) were adopted for areas thought to have more friction because of a longer or rougher path and larger k_1's for trajectories with lesser probable friction.

A k_1 of 0.40 was used for all Coast Range com-

putations, except at point J (shown on fig. 24) where 0.25 yielded more consistent outflows and is justified on the basis of rough terrain.

Unsaturated layers. Most of the air along ascending trajectories was saturated. Along the southern boundary of the analysis area the lower layers were unsaturated. To circumvent the programming complexity of finding the condensation level and working with two different ascent lapse rates the program was set up for all ascent to be at the moist adiabatic lapse rate. For unsaturated inflow air the wet-bulb temperature T_1' (fig. 17) was substituted for the inflow temperature T_1. An adjustment ΔA, to the energy area, A, was determined manually on an adiabatic chart (fig. 17) and introduced as part of the inflow data. The energy equation for unsaturated air was then, from equation (6),

$$\frac{1}{k_3}(V_4^2-V_3^2)-\frac{1}{k_1}(V_2^2-V_1^2)=2R(A+\Delta A)+F \tag{12}$$

where A is the energy area based on T_1' and ΔA the correction.

Level flow. For essentially level flow at lower levels, for example the trajectories terminating at Red Bluff, the principles which determine the "outflow" profile of speed, temperature, and pressure for any given outflow surface wind speed, V_2, apply equally as well as over a ridge. That is, equations (6) and (10) and the laws of adiabatic temperature variation still apply. Sets of machine computations of outflow profiles were made in exactly the same manner as for ridge points. However the minimum energy method of selecting the valid outflow profile from the set computed (step 7, page 19) does not apply to the level flow situation. There is no obstruction that offers a control on the flow, in the sense that "control sections" exist in water flow. The control comes from friction and from other effects analogous to water flow in a channel other than at a control section.

At Red Bluff, the observed surface wind and pressure and the empirically determined winds up to about 900 mb. were accepted. Winds at higher levels that were dynamically consistent with them were then found by selecting a dynamically computed outflow profile which in the lower levels fits the other data. To accomplish this, the friction coefficient, k_1, and the depth of the friction layer were adjusted. A fit was obtained

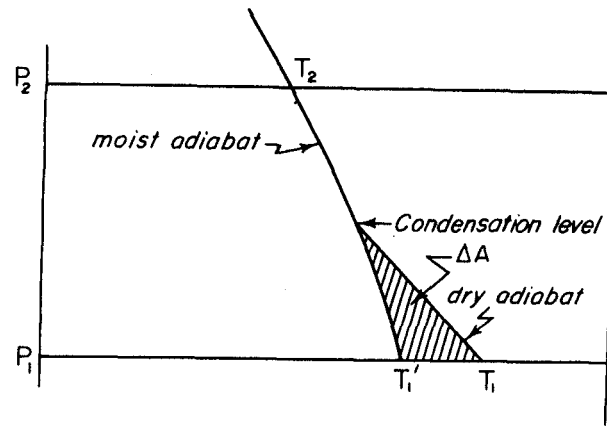

FIGURE 17.—Adjustment ΔA made for unsaturated inflow air to avoid using two ascent lapse rates in the numerical computations.

at Red Bluff with k_1 of 0.15 and a depth of friction layer of 0.15 p_r, instead of the 0.1 p_r used elsewhere. (See [2], Section 3.) p_r is the surface pressure. It is not known why a higher friction value (lower coefficient) is obtained for the valley flow to Red Bluff than for the ridge flow to Blue Canyon.

Computations of speeds at mid-valley point 39°30′ N., 122° W. were made in the same manner as at Red Bluff, except that k_1 was increased to 0.25 in view of the shorter path.

APPLICATION OF DYNAMIC COMPUTATION METHOD

Computation points. To find the distribution of temperature, pressure, and wind speed on the mountain slopes and ridges a number of computation points were chosen in these areas. In addition, three points were chosen in the northern Central Valley, Mt. Shasta, Red Bluff, and the point 39°30′ N., 122° W. Figure 18 shows the location of the computation points (18 in all), and the surface and "500-mb." trajectories terminating at these points. The latter in the figure are the final trajectories which cross through the 500-mb. surface at the initial or inflow entrance point. However the horizontal projection of the initial tentative trajectories was very close to the same in all cases. Three of the 18 computation points coincide with weather reporting stations—Red Bluff, Mt. Shasta, and

690-385 O—63——4

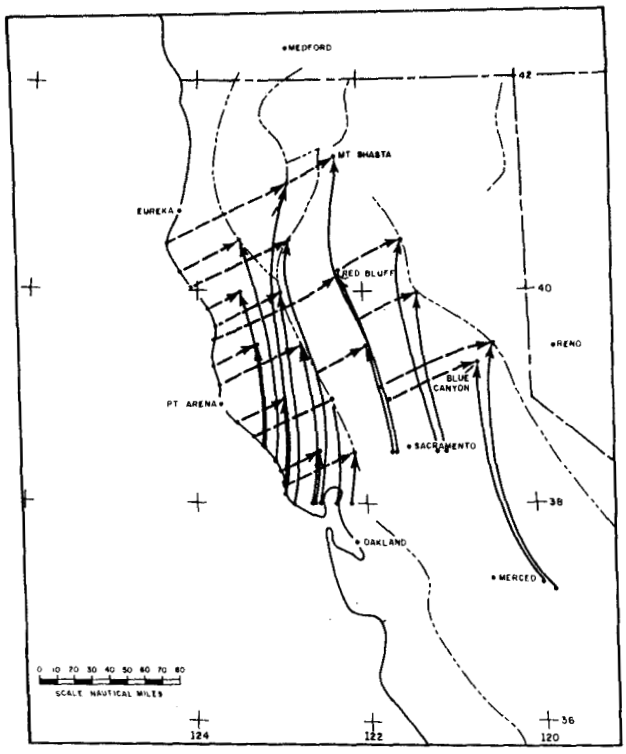

FIGURE 18.—Computation points and the surface (solid) and "500-mb." (dashed) trajectories terminating at these points (18 in all).

Blue Canyon. In these cases the outflow surface pressure, temperature, and wind are known quantities.

Entrance data. The entrance data for the coast ridge computations were scaled from a cross section along the coastline (represented by straight-line segments connecting Eureka, Point Arena, and Oakland) and along the 38th parallel (the latter about 15 miles north of Oakland), shown in figure 19. The outflow at the ridge crest was in turn used for input for the upper levels of the Central Valley computations; lower-level input was scaled from an east-west cross section at 38°30′ N. (near Sacramento). Finally, data from the center line of the Central Valley were used for input to the Sierra Nevada trajectory computations. For the trajectories terminating at Blue Canyon and on the adjacent Sierra ridge line it was necessary to take the surface and the lower-level input far to the south in order to start at a low elevation.

Input data were read off the cross section auxiliary maps (or directly from data) for the following levels:

1000 mb. or top of inversion		
950 mb.	400 mb.	150 mb.
900 mb.	350 mb.	140 mb.
800 mb.	300 mb.	130 mb.
700 mb.	245 mb.	110 mb.
600 mb.	200 mb.	100 mb.
500 mb.	160 mb.	80 mb.

Along the coast the top of the surface inversion was chosen as the bottom computation level. This was quite close to 1000 mb. at 38° N. and 980 mb. in the north. The thin layer below the inversion (of about 20 mb.) was ignored, following [2]. Elsewhere computations generally started at 1000 mb., very near the ground.

Computations. Vertical soundings of wind speed, temperature, and pressure were computed for each of the 18 computation points with a digital-electronic computer. In each instance steps 1 through 8 at the beginning of this section for two-dimensional wind flow were followed, with the substitution of equation (10) for equation (2), and equation (12) for (1).

The computed outflow pressures were compared with the assumed pressures on the tentative trajectories. Where there was sufficient difference to change the horizontal projection of the revised (3-dimensional) trajectory appreciably (i.e., change the inflow point), a new determination was made. This was required at only a few points.

Some special problems are discussed in later paragraphs.

RESULTS OF DYNAMIC COMPUTATION METHOD

Temperature and wind. The result of each dynamic computation is a temperature and wind sounding, located at a computation point.

a. Temperature soundings

The soundings developed by these methods show reasonable and for the most part expected results. Heights and analyses based on these soundings give intelligible results. Figures 20, 21, and 22 show the soundings for a Coast Range point, F; a valley point, Red Bluff; and a Sierra ridge point, M. (Figure 24 shows the location of the computation points.) Lapse rates are for the most part near moist adiabatic except in the

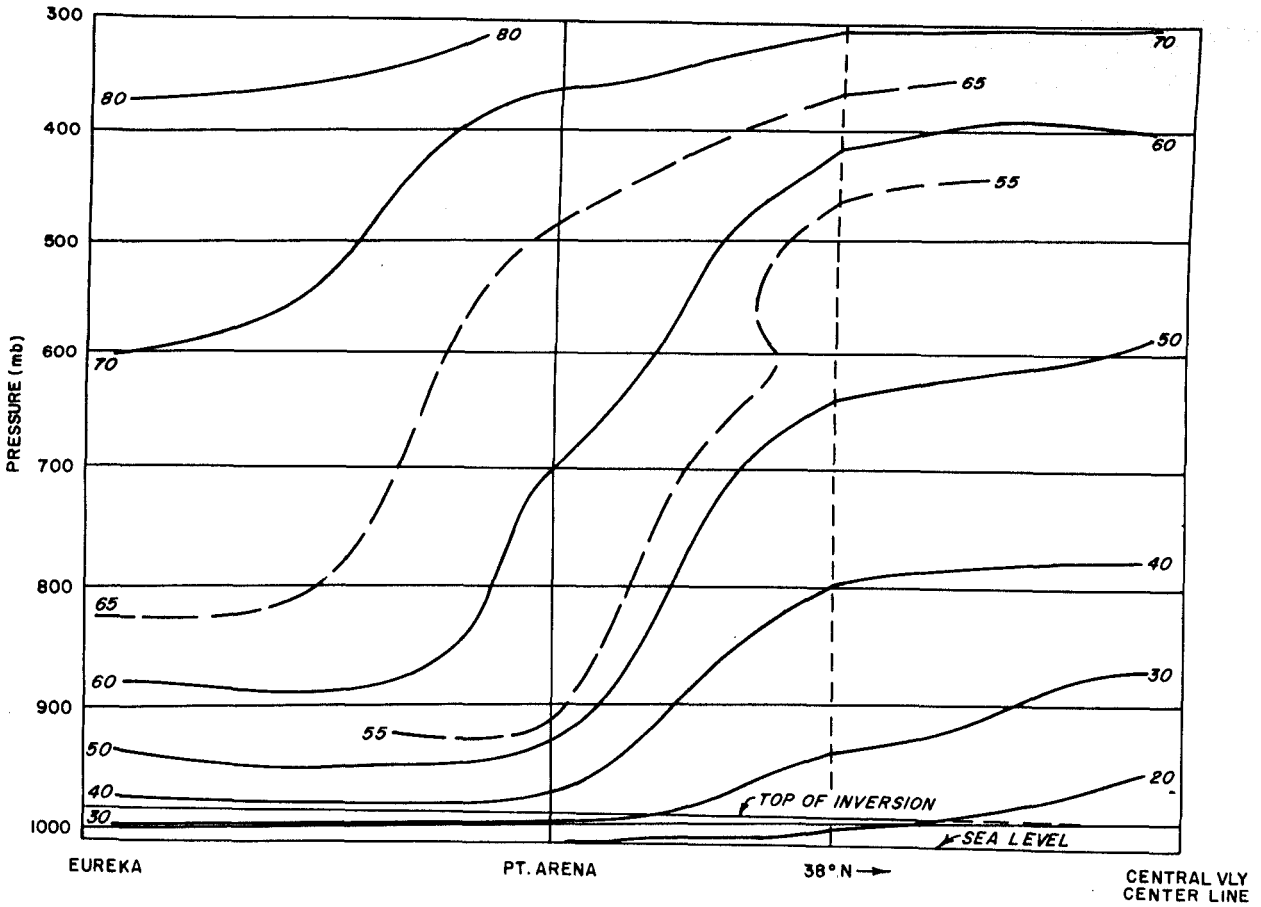

FIGURE 19.—Cross section of temperature and pressure values along coastline (straight-line segments from Eureka to Point Arena to Oakland) and thence along 38° N., from which input values were read for computation points on Coast Range ridges (see fig. 18).

lowest 50 mb. For coastal computation points the low-level air is cool and moist, being directly from the ocean. The Sierra low-level air, on the other hand, rises from the Valley floor to the south of San Francisco Bay having originally come over the Coast Range at the southern end of the Central Valley. For this reason the air is drier before lift. The lapse rate of the lifted air as shown by the Sierra ridge point M (fig. 22) has an inversion of about 1.5° at the surface. This inversion existed in the non-saturated Valley air and was not destroyed by the lift. The Coast Range sounding (fig. 20) shows an unstable lapse rate in the lowest layers. That is, air is saturated with lapse rate greater than the moist adiabatic. This comes about because the low-level air comes from much farther south than the air at the intermediate levels. Since the air is saturated (or assumed so) at all levels, the air from farther south retains its warmth relative to the upper layers even though it is lifted farther. This gives a clue to the exceedance of Coast Range observed precipitation, ascribed to convection, over that computed from laminar flow.

The Central Valley temperature soundings show the lower layers to be nearly isothermal. Subsidence above 980 mb. accounts for this low-level warm air.

b. Wind soundings

The calculated vertical distribution of the wind above the mountain cannot be verified directly.

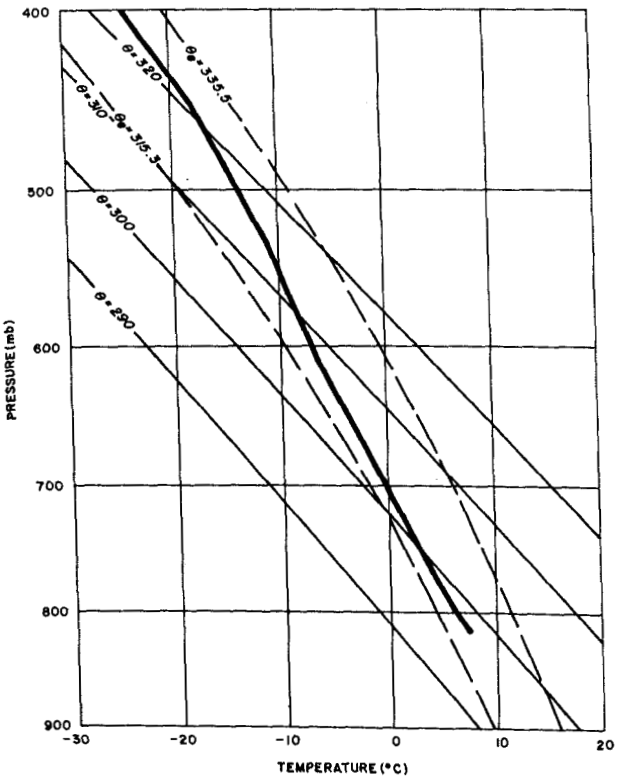

FIGURE 20.—Temperature sounding constructed for computation point F on the Coast Range ridge. (See fig. 24 for location.)

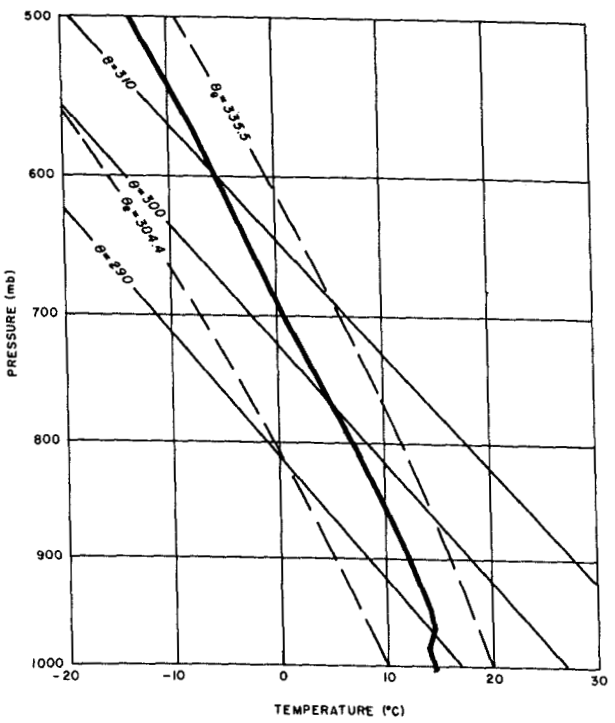

FIGURE 21.—Temperature sounding constructed for computation point Red Bluff in the Central Valley. (See fig. 24.)

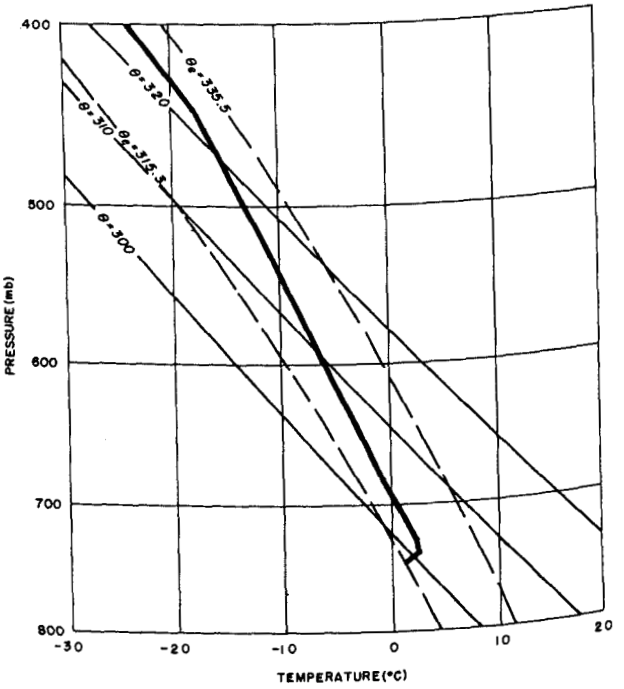

FIGURE 22.—Temperature sounding constructed for computation point M on the Sierra Nevada ridge. (See fig. 24.)

The wind profiles derived by this theory seem quite reasonable, however, and fit the facts as far as they are known. A sample of inflow and outflow wind profiles for Sierra ridge point N (at 40° N.) is shown on figure 23. The inflow profile is dashed, and arrows show the lift to outflow. Surface outflow speed is 32.5 kt., a reasonable figure for that region. A very pronounced increase in wind through the friction layer culminating in a peak about 2000 ft. above the surface is revealed. Most of the ridge soundings observed by aircraft or from balloon observations exhibit this characteristic [8]. Winds above this level to the nodal surface show the expected speed increase over inflow that reflects the acceleration needed to draw the air over the mountain ridge. Well above the nodal surface, where the air is descending and moving toward higher pressure, deceleration occurs.

Sea level pressure. The computed outflow sounding gives the surface pressure at the ridge point. The surface pressure is a measure of the pressure drop required to accelerate the air over the ridge. The effect of this pressure drop in increasing V^2 is proportional to $\ln (p_2)_h - \ln p_2$,

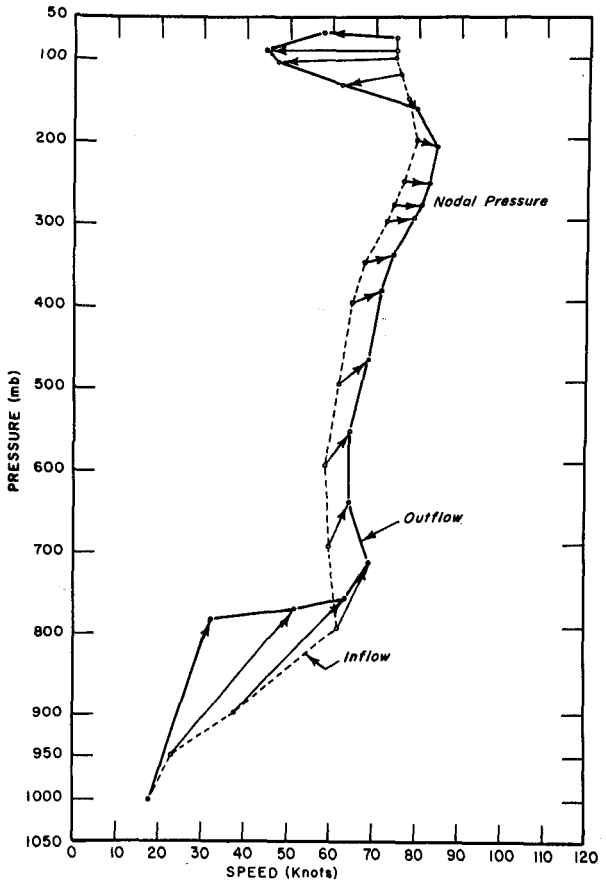

FIGURE 23.—Wind profiles (inflow dashed, outflow solid) derived for computation point N on the Sierra ridge. (See fig. 24 for location.)

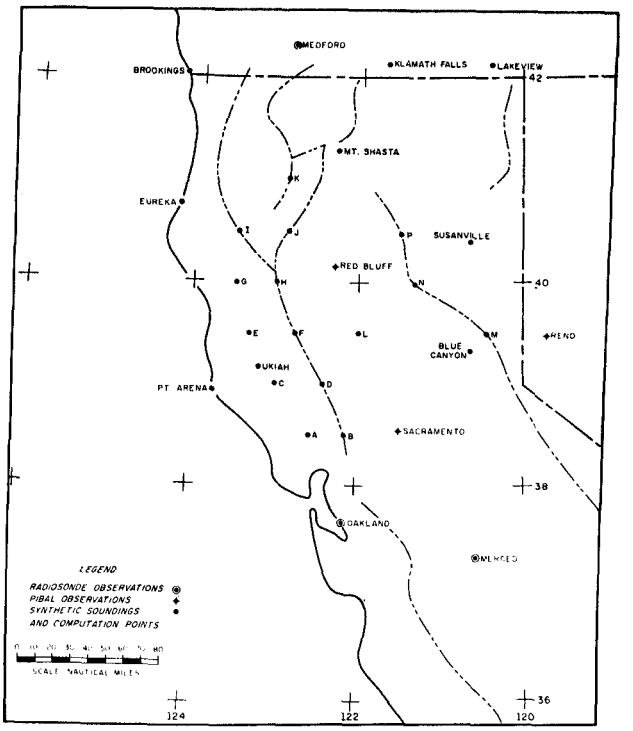

FIGURE 24.—Computation points, synthetic soundings, pibal and raob stations which provided the network for the contour analyses.

where the symbols have the meaning of equation (11). To depict this effective pressure drop on a sea level chart the sea level pressure at the ridge crest is computed from

$$\ln (p_1)_{SL} - \ln (p_2)_{SL} = \ln (p_2)_h - \ln p_2 \qquad (13)$$

where $(p_1)_{SL}$ is the sea level pressure at the entrance point of the surface streamline and $(p_2)_{SL}$ is the sea level pressure at the ridge crest. The application of equation (12) to solve for $(p_2)_{SL}$ is equivalent to reducing p_2 to sea level by the hypsometric formula, using the temperatures along the surface streamline as the virtual temperatures of the column. The computed sea level pressures are shown on figure 9.

It is interesting to note that p_2 (and therefore $(p_2)_{SL}$ also) is dependent on the entire flow, when the outflow is computed by the steps on pages 18–19, and is not sensitive to the surface friction coefficient. This was demonstrated by computing sets of outflows in which only the surface friction coefficient varied. It was found that equation (11) was satisfied for changes in k_1 by an almost compensating change in V_2, and that p_2 was but slightly affected.

Constant pressure charts. Constant pressure charts were constructed for nine levels from 1000 to 300 mb. inclusive based on computations for the network shown in figure 24. Seven are presented in figures 25–31. The data upon which the immediate coastal portion of the constant pressure charts were based came directly from composited real and synthetic soundings. The contours over the Coast and Sierra ranges as well as over northern portions of the Central Valley were derived from the theoretical temperature soundings discussed above.

It will be noted that these charts differ in one major respect from ordinary constant pressure

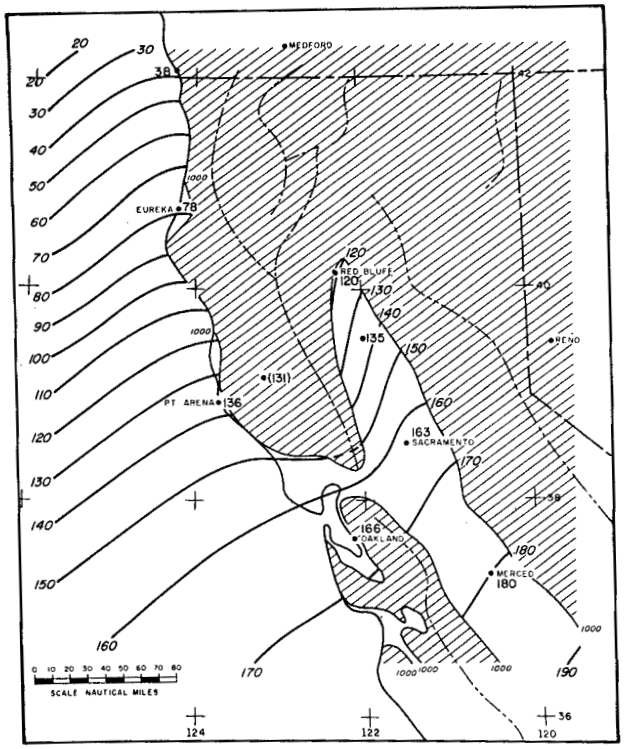

FIGURE 25.—Contours (m.) constructed for 1000-mb. surface from composited observed and synthetic soundings and theoretical temperature soundings. In this and the following maps, shading shows terrain higher than the level of interest. Values in parentheses are heights very slightly below ground level.

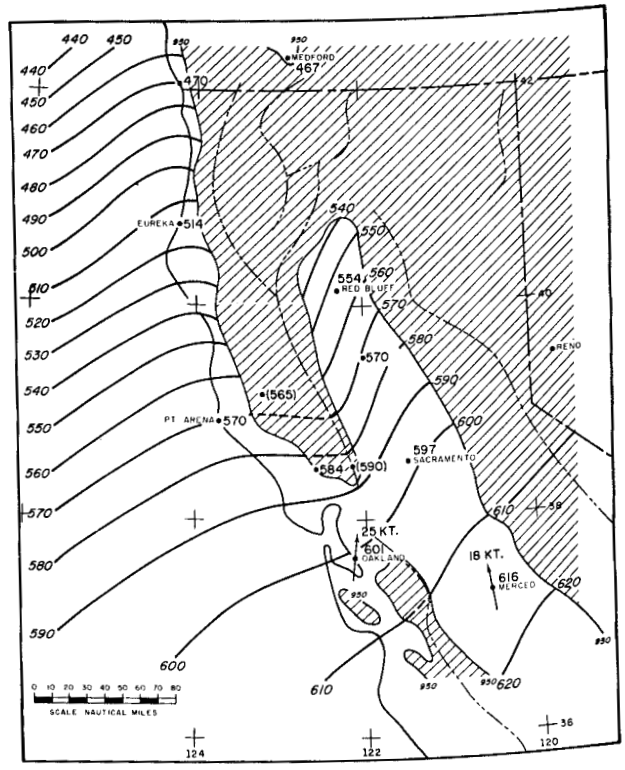

FIGURE 26.—Contours (m.) constructed for 950-mb. surface.

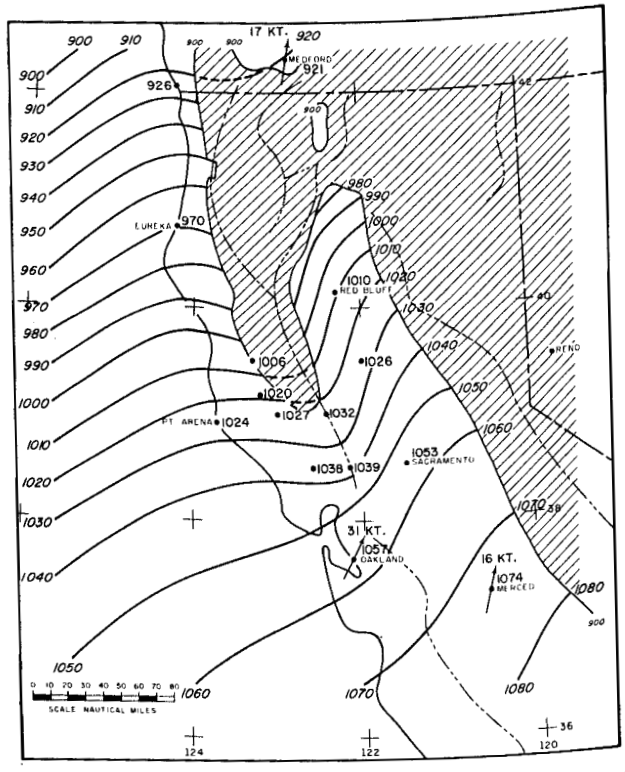

FIGURE 27.—Contours (m.) constructed for 900-mb. surface.

charts, namely, the troughs in the height contours over the mountain ranges and generally elevated land. These contour troughs are present whenever the inflowing air is initially stable. Upon being lifted, the air is cooled below the surrounding free-air temperatures forming a trough that increases in intensity with height up to the nodal surface. An important related factor is the essential nature of this trough if air is to be drawn over the mountain range, since acceleration is required if continuity of mass is to be preserved. That is, the air must move toward low pressure. It might be pointed out that this trough has not been observed but is based on deductions from given conditions and the observed fact that the air does cross the mountains.

It should not be inferred that the pressure troughs over the ranges are as pronounced as this most of the time. The selected storm period was one of very pronounced cross-ridge flow, in

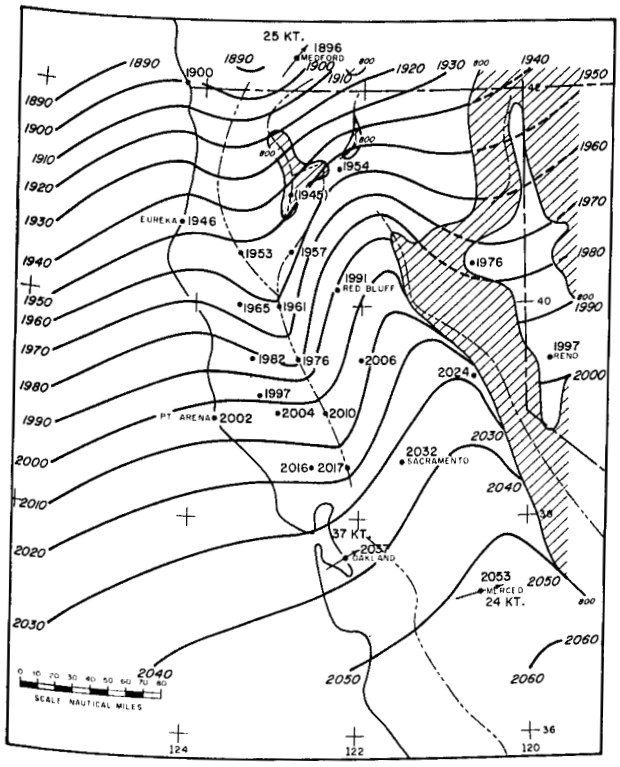

FIGURE 28.—Contours (m.) constructed for 800-mb. surface.

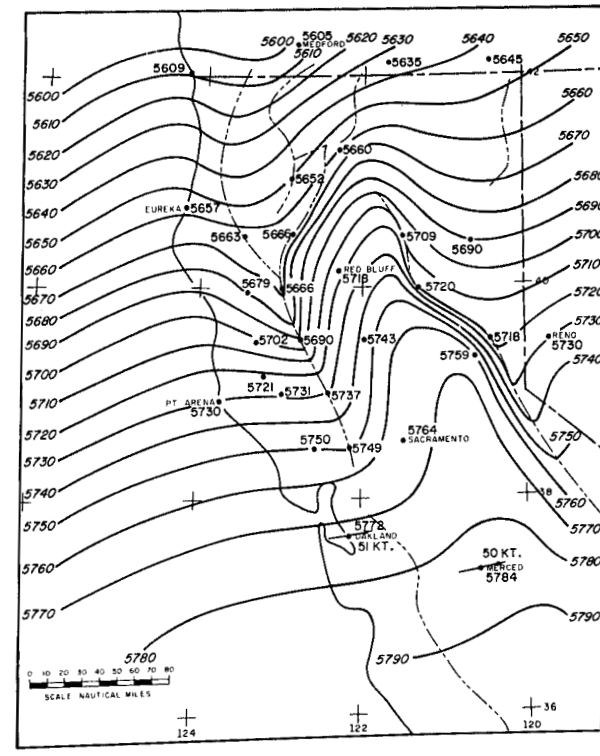

FIGURE 30.—Contours (m.) constructed for 500-mb. surface.

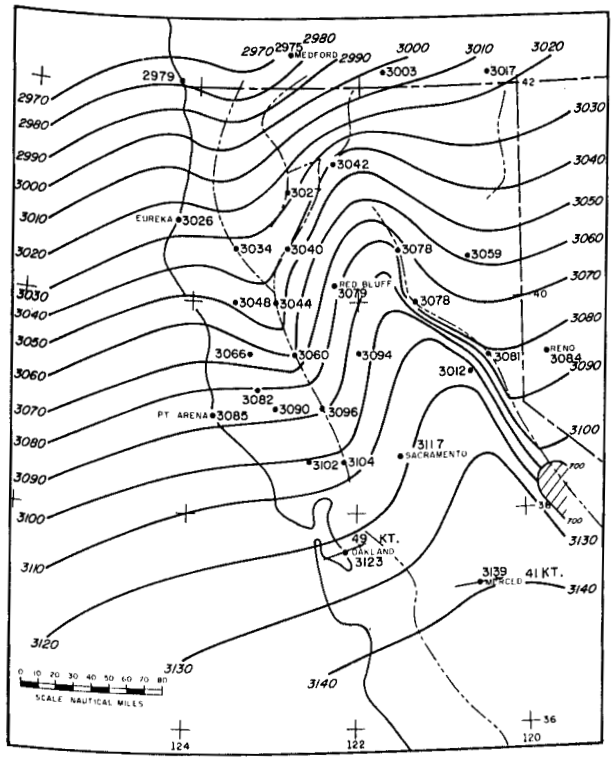

FIGURE 29.—Contours (m.) constructed for 700-mb. surface.

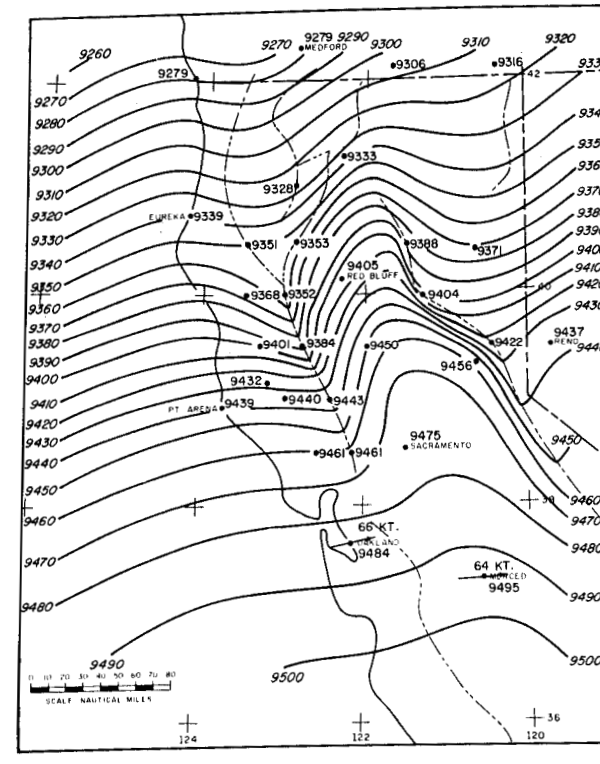

FIGURE 31.—Contours (m.) constructed for 300-mb. surface.

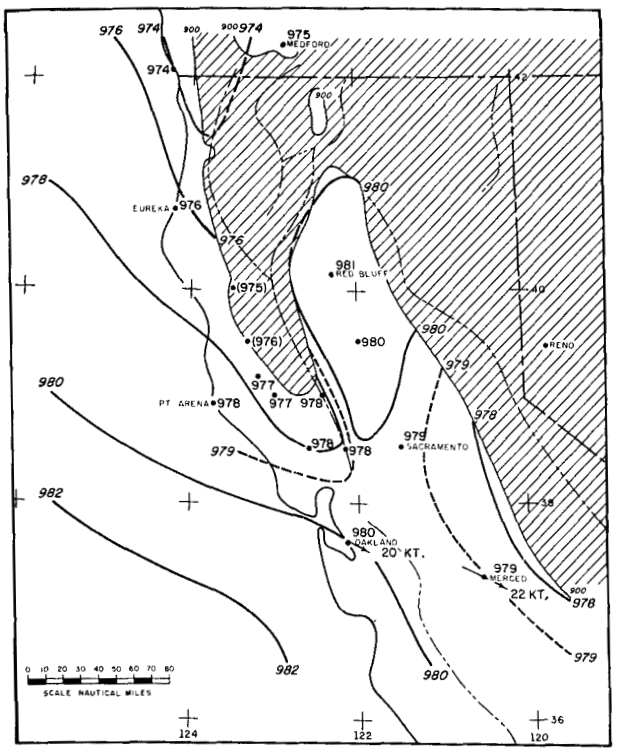

FIGURE 32.—Composited thickness (m.) chart for layer 900 to 800 mb. Shading covers terrain higher than 900 mb.

comparison with storms of usual magnitude. This is inferred from the heavy precipitation and from the strong north-south pressure gradient at all levels. The Sacramento-Red Bluff sea level pressure difference is the largest of record for all durations from 6 to 72 hours during this general storm, though not necessarily synchronous with the 24-hour composite period. (See fig. 5–17, [6].)

Thickness charts. Thickness charts were constructed for all layers from 1000–950 mb. to 500–300 mb., inclusive. These served not only as a consistency check on the synthetic soundings, but also provided additional constant pressure heights for use where surface pressure observations were available. Thermal winds computed from the observed winds were of aid in the analysis of the thickness charts. Additional thickness values were derived from virtual temperatures along the streamlines used for rainfall computations. Figure 32 shows a sample composited thickness chart (for the 900–800-mb. layer).

Locus-of-airflow contour charts. The three-dimensional airflow is summarized in special contour charts in figures 33 through 40. Figure 33, for example, is a locus-of-airflow chart for 950 mb. The contours on the chart depict the pressures through which the air rises or falls after it crosses either the coast or the 38th parallel at 950 mb. The three-dimensional trajectories lie within the locus-of-airflow surface. The curves with arrow heads are the horizontal projection of the three-dimensional trajectories that "enter" at 950 mb. The surface streamline chart, figure 10, is also a member of the locus-of-airflow family. The locus-of-airflow charts were the basis for the precipitation computations described in the next section.

The locus-of-airflow charts were constructed by interpolation from the computed three-dimensional trajectories by reference to the ground elevations. Over the lower parts of the Coast Range, where the minimum-energy hypothesis does not exercise as positive control as over higher ridges, some smoothing of the specific pressures on the computed trajectories was introduced.

One interesting feature of the locus-of-airflow charts is that there is an area in the Central Valley north of Sacramento in which the air descends to a lower elevation than its entrance pressure, at 950 mb. and again at all levels from 850 mb. upward. At 500 mb. this "lower than entrance" area has spread over the entire valley floor area and onto the foothills on both sides of the valley. There is continued growth upward and at 300 mb., figure 40, the air is lifted over only the highest part of the Coast Range and over the Sierra range where the crest is 8000 ft. (750 mb.) or higher.

The Mt. Shasta problem. For the trajectory terminating at Mt. Shasta the inflow surface wind speed was higher than the outflow observed composite surface wind speed. The particular manner in which friction is introduced into the calculations [2] is not designed to handle a decrease in speed along the streamline; a very large frictional value tends to make V_2 approach, but not become less than V_1. To take care of this without undue complexities in the machine program, outflow data at Mt. Shasta were computed with a friction coefficient, k_1, of 0.05, which yielded both too high a surface wind and too low a surface pressure. The surface wind and pressure were set at the observed values and the rest of the computed profile subjectively modified to conform to the surface data.

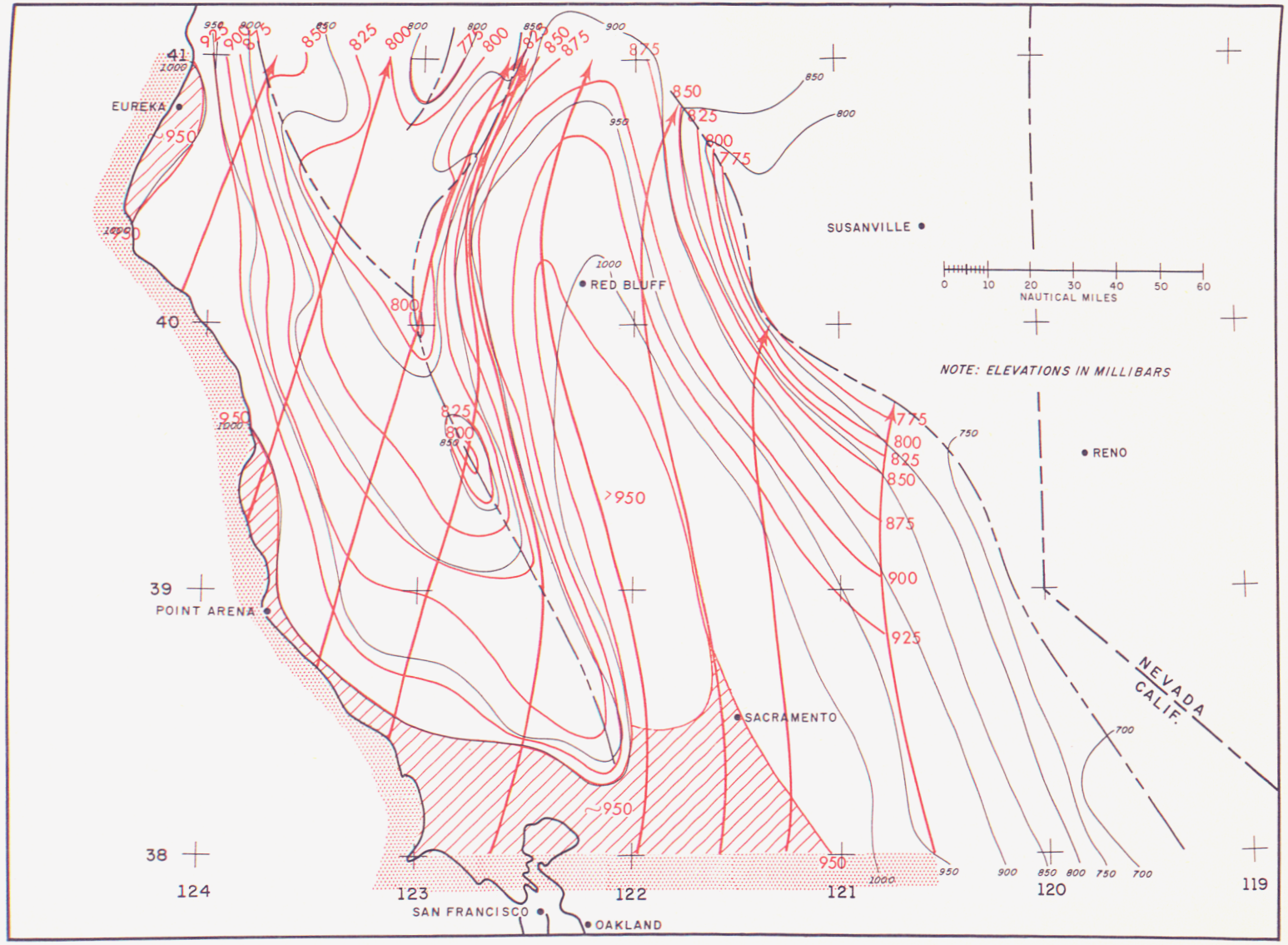

FIGURE 33.—Locus-of-airflow chart for 950 mb. Contours (labeled in mb.) show pressures through which air rises or falls after it enters the study area at the 950-mb. level and follows the trajectories of the arrowed curves. Shading indicates areas over which air is relatively undisturbed from entrance pressure level.

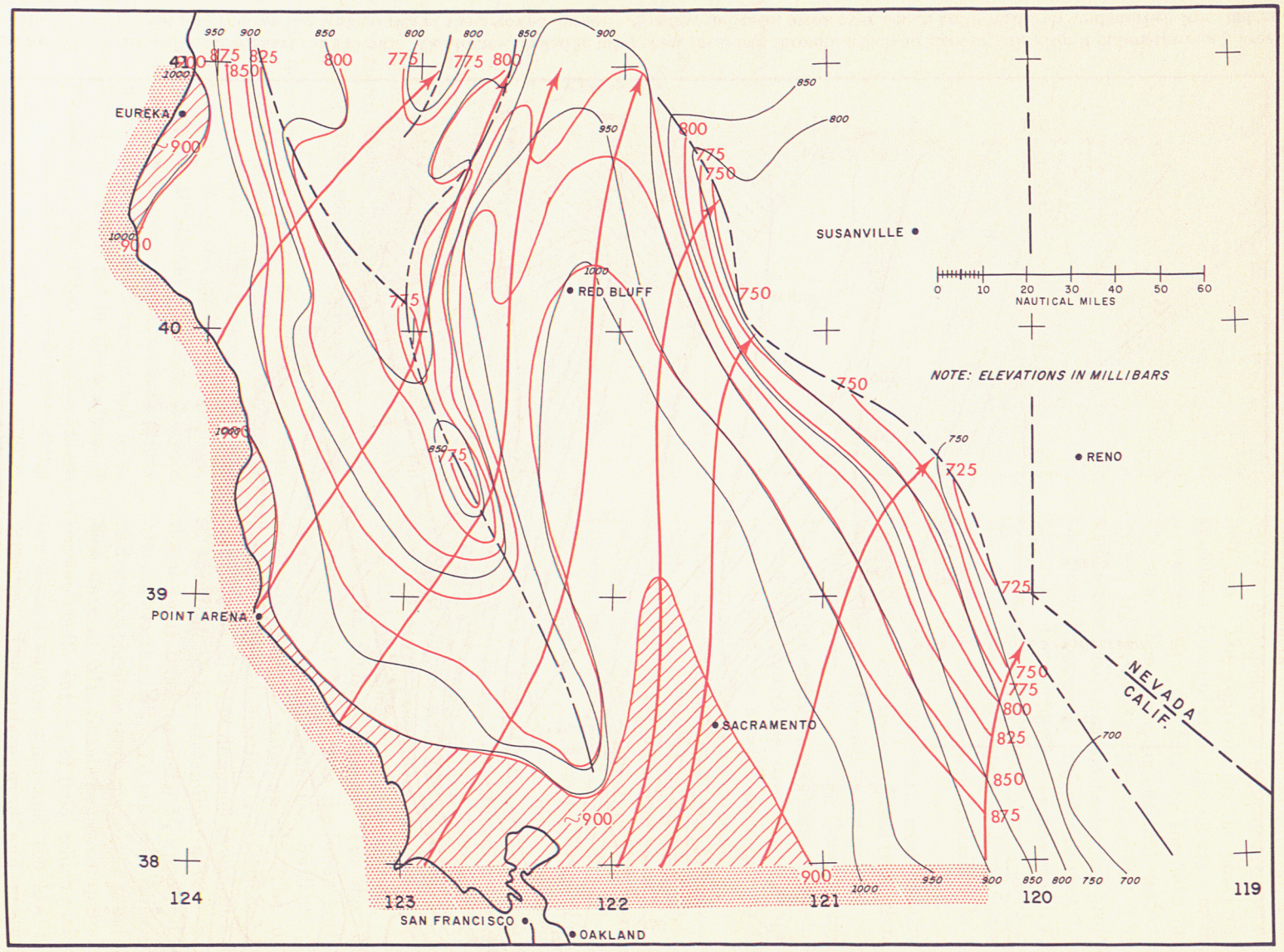

FIGURE 34.—Locus-of-airflow chart for 900-mb. entrance level.

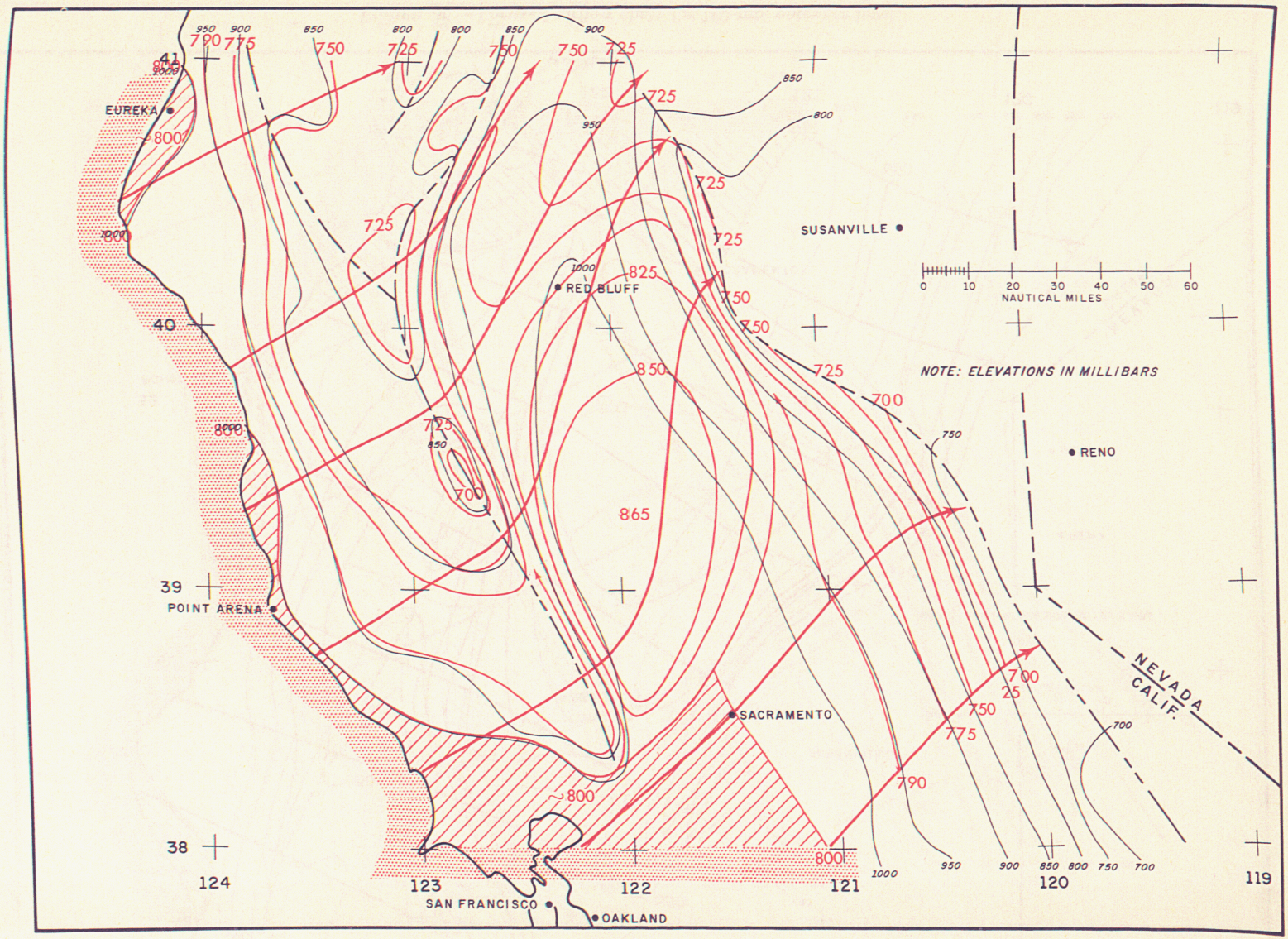

FIGURE 35.—Locus-of-airflow chart for 800-mb. entrance level.

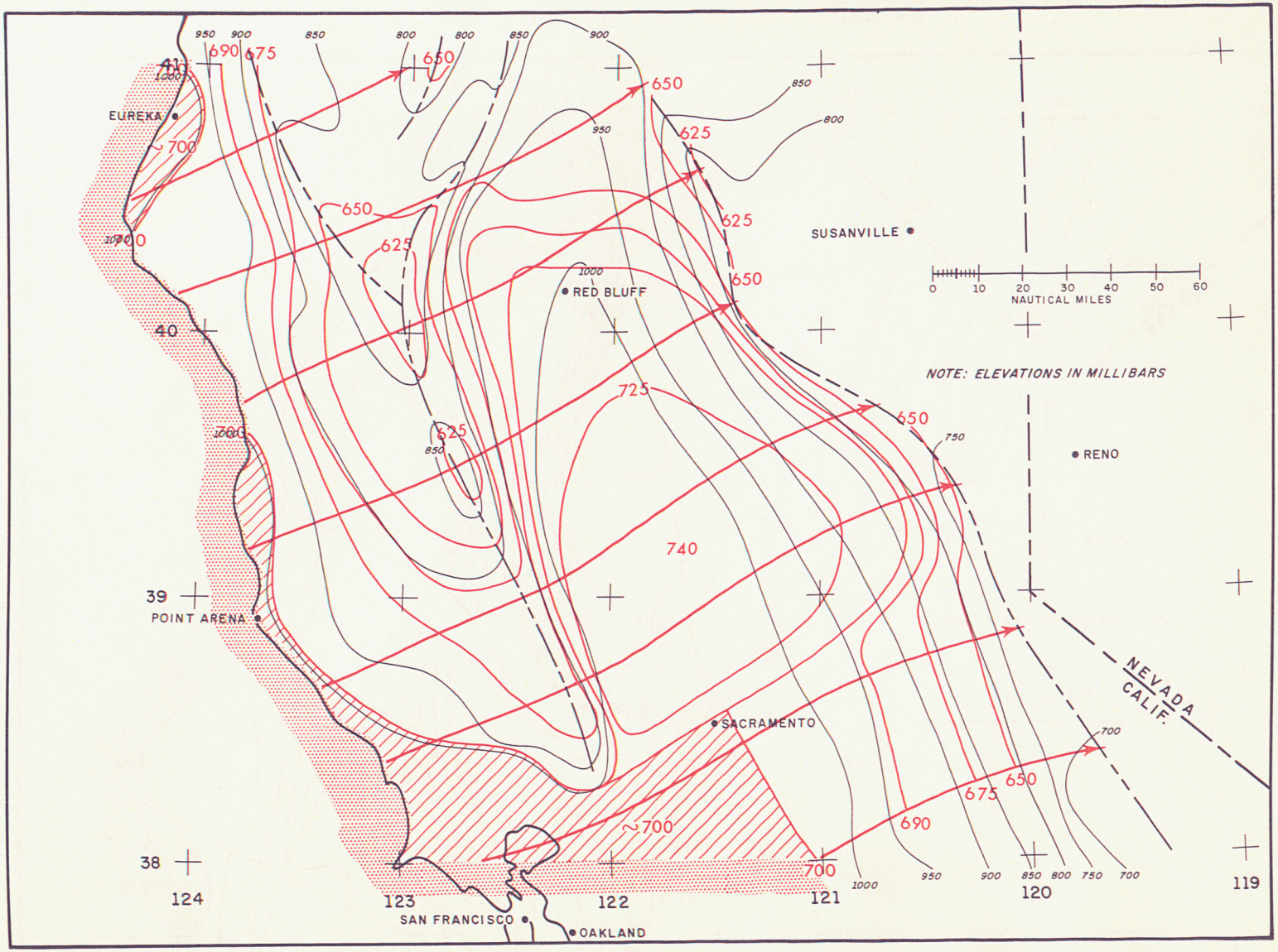

FIGURE 36.—Locus-of-airflow chart for 700-mb. entrance level.

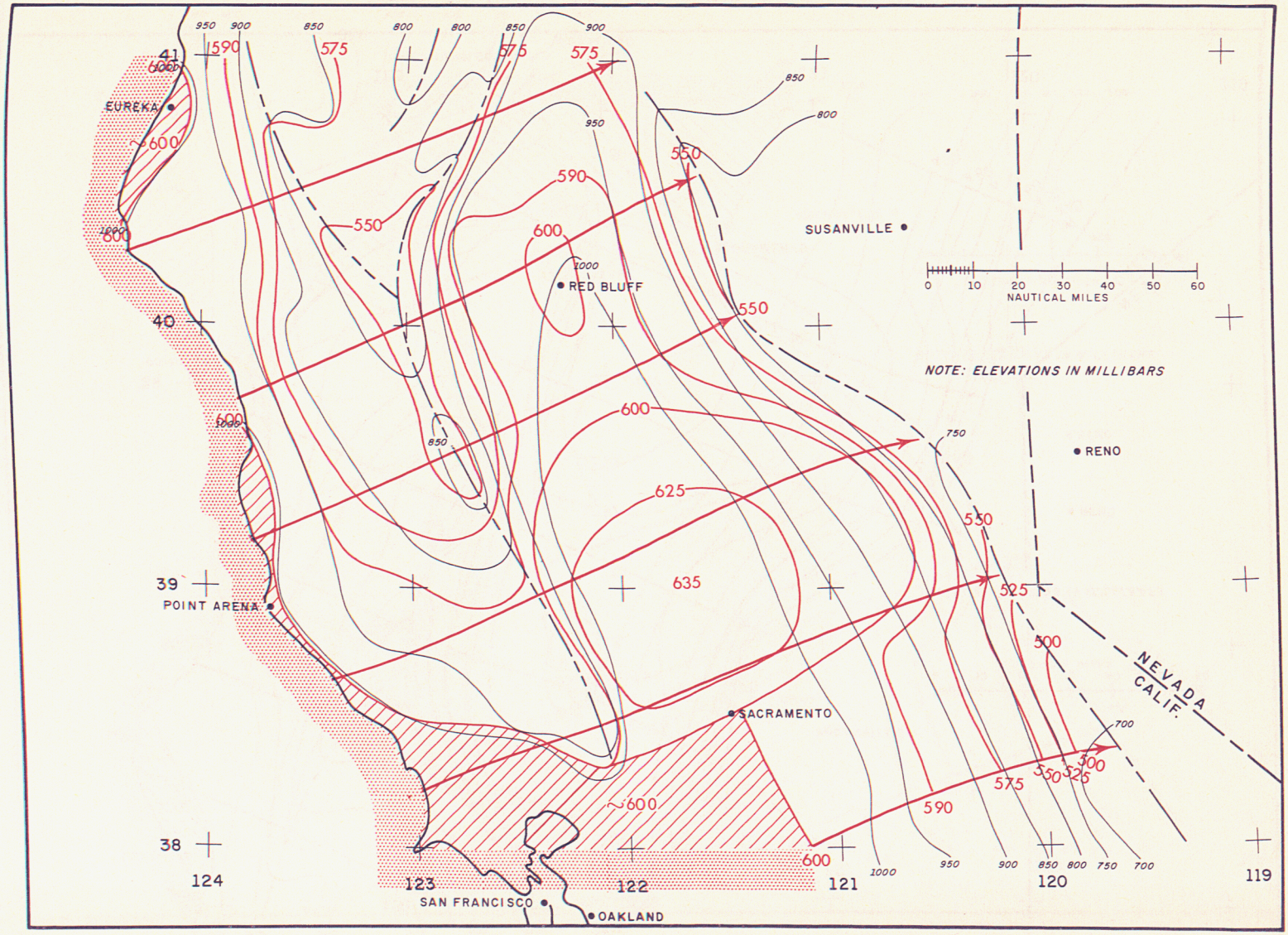

FIGURE 37.—Locus-of-airflow chart for 600-mb. entrance level.

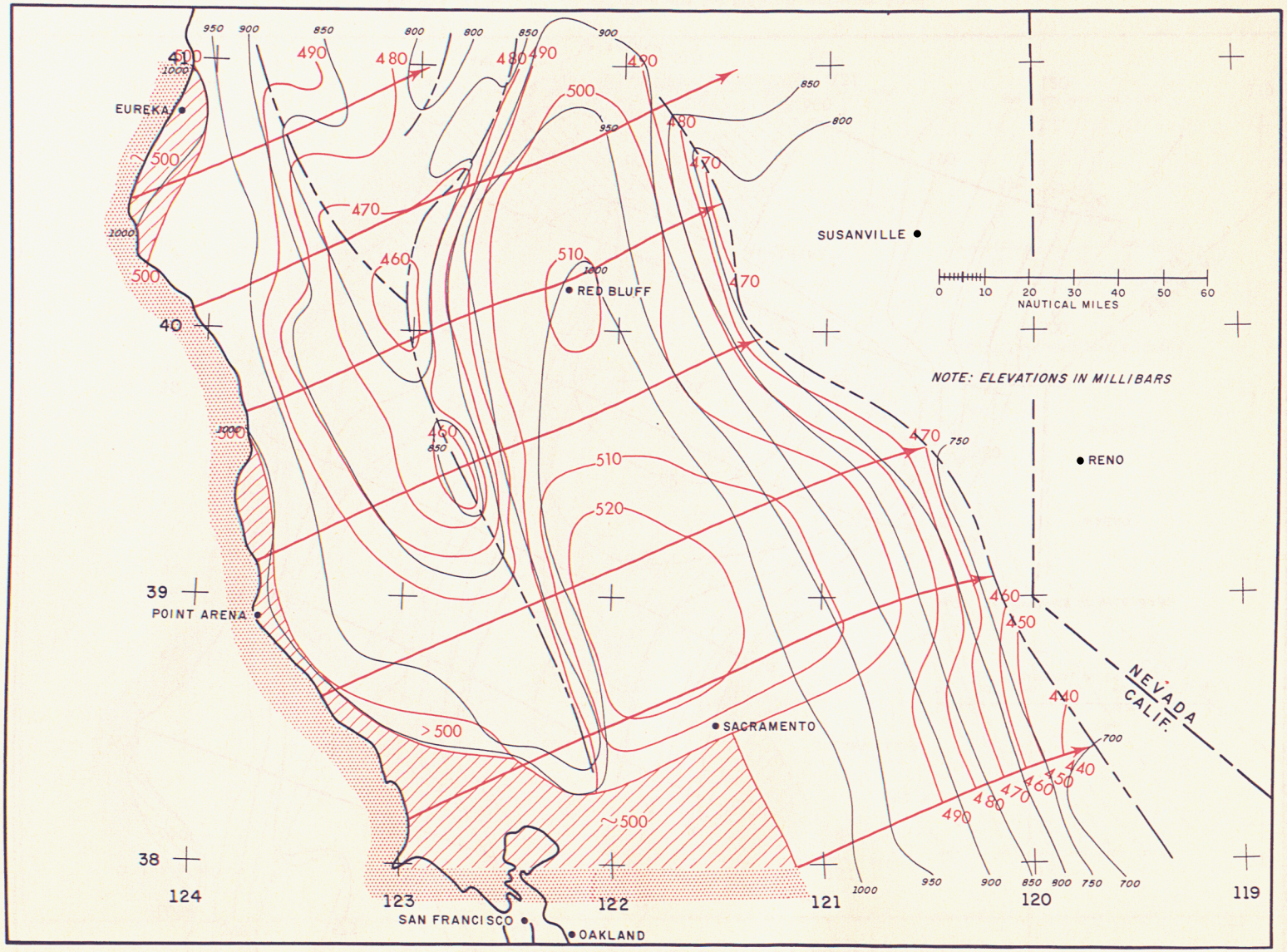

FIGURE 38.—Locus-of-airflow chart for 500-mb. entrance level.

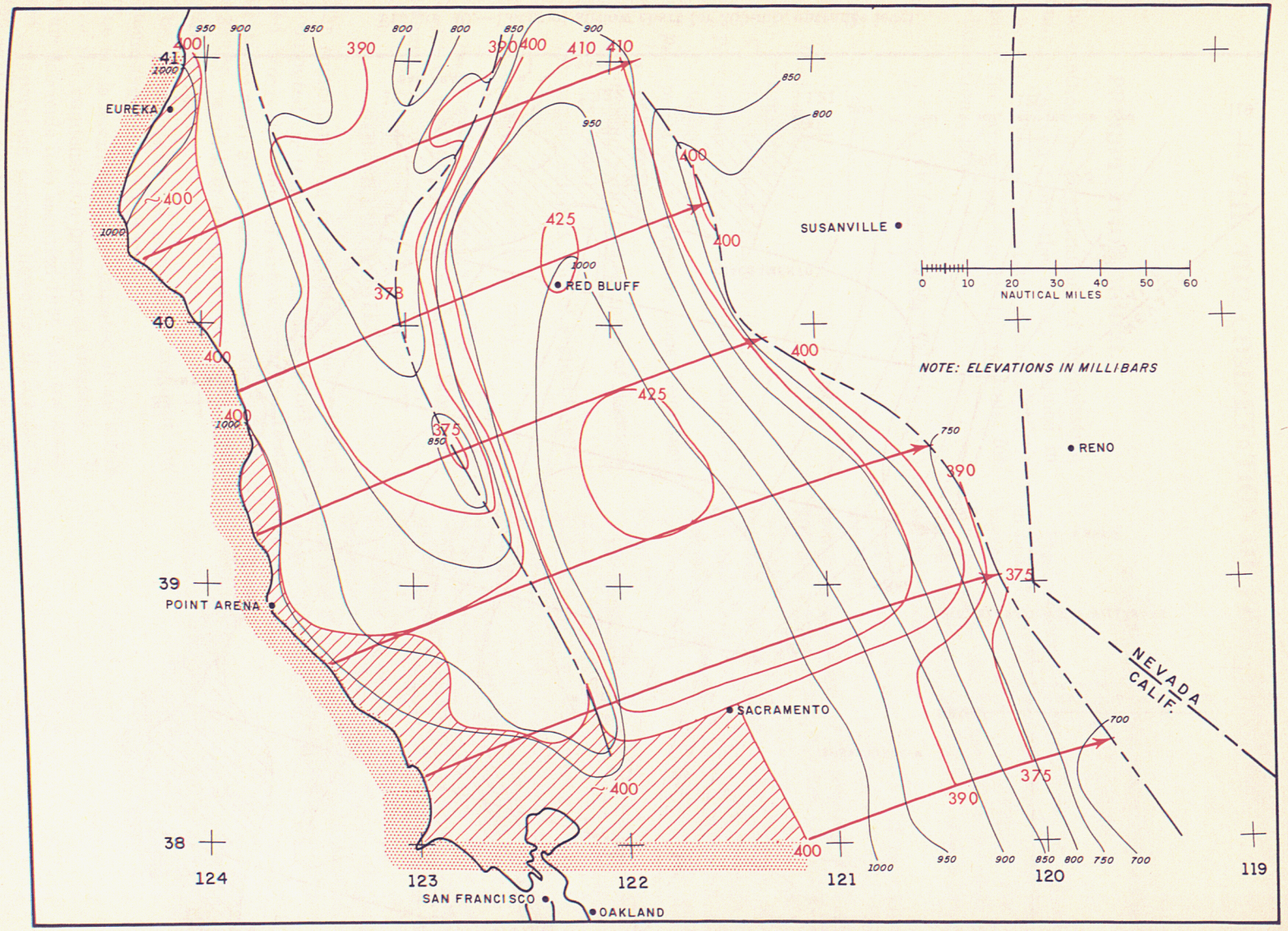

FIGURE 39.—Locus-of-airflow chart for 400-mb. entrance level.

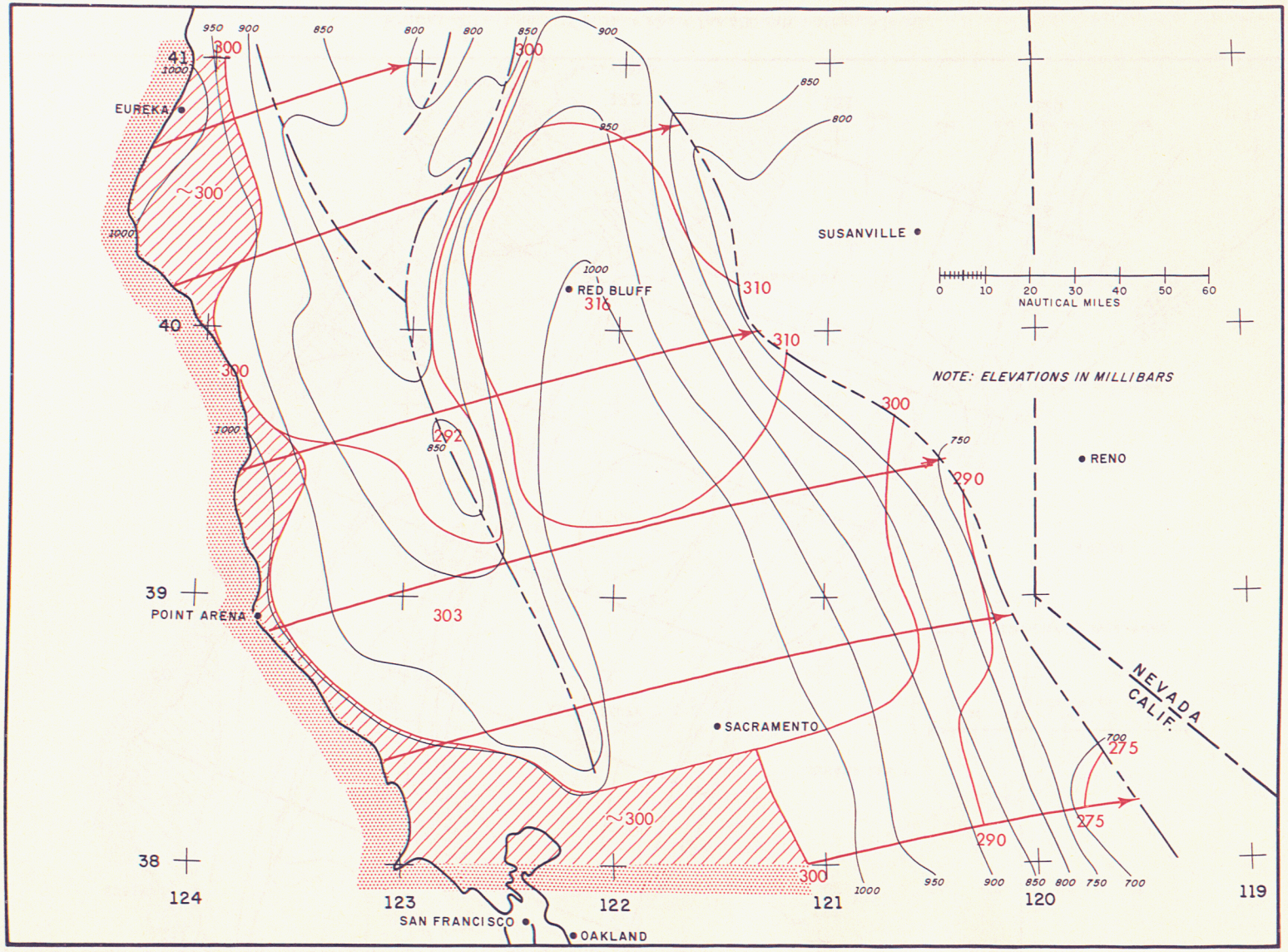

FIGURE 40.—Locus-of-airflow chart for 300-mb. entrance level.

VIII. THE COMPUTATION OF PRECIPITATION

PRECIPITATION MODEL

The method of computation of precipitation amount is derived from the theory outlined in [6] (p. 54). The precipitation intensity (I) is computed for layer segments by the formula, for two-dimensional flow

$$I=\frac{R}{t}=\frac{.4V_i(p_{el}-p_{eu})(q_a-q_b)}{Y} \qquad (14)$$

where

R=rainfall (in.)
t=time (hr.)
V_i=the air speed at inflow (kt.)
p_{el}=pressure at entrance, lower boundary of layer (mb.)
p_{eu}=pressure at entrance, upper boundary of layer (mb.)
q_a=mixing ratio at beginning of segment (gm./gm.)
q_b=mixing ratio at end of segment (gm./gm.)
Y=length of segment (n. mi.)

$p_{el}-p_{eu}$ therefore represents the layer thickness and q_a-q_b the decrease in moisture along the segment.

AIR TRAJECTORIES

The computation of precipitation makes use of the computed air trajectories and additional ones scaled from the locus-of-airflow charts. These trajectories start at entrance lines along the coast, the 38° N. parallel, or along the center-line of the Central Valley.

The precipitation is computed segment by segment along the trajectory.

The air is assumed to be saturated at all levels above the condensation pressure at entrance. If the air descends it is assumed that half the maximum evaporation occurs; however, if the air is lifted again after a period of descent no allowance is made for descent drying; that is, 100 percent recharge of the air by evaporation is assumed.

MECHANICS OF PRECIPITATION COMPUTATION

Precipitation is computed for the layers given in table 2. The upper and lower boundary of the layer are at inflow or entrance. For coastal computations, the bottom layer is taken between the inversion top and 975 mb. and is therefore of variable thickness.

Raindrops are assumed to fall at a rate of 36 mb./min., while the snow rate is 0.21 times the rain rate (from [6]). The freezing level, at about 700 mb. in this storm, divides the rain and snowfall rates. The precipitation is assumed to move forward with the wind. Combination of rate of fall and wind speed give a drift distance which is defined as distance that precipitation elements move forward while falling from top to bottom of layer.

The accumulated precipitation at the bottom of each layer is moved forward (drifted) with the drift distance of the layer below it and added graphically to the precipitation at the bottom of that layer. Only the "positive" precipitation is moved forward into the succeeding lower layer, as the "negative precipitation", or evaporation, operates only in its original position. Within each layer, however, the evaporative power along a descending segment consumes a part of the precipitation falling through. Figures 41 and 42 show examples of calculated layer precipitation and the accumulation of precipitation in two layers.

TABLE 2.—*Layers for which precipitation was computed.*

Layer (mb.)	Thickness (mb.)
1000–975	25
975–925	50
925–850	75
850–750	100
750–650	100
650–550	100
550–450	100
450–350	100
350–250	100

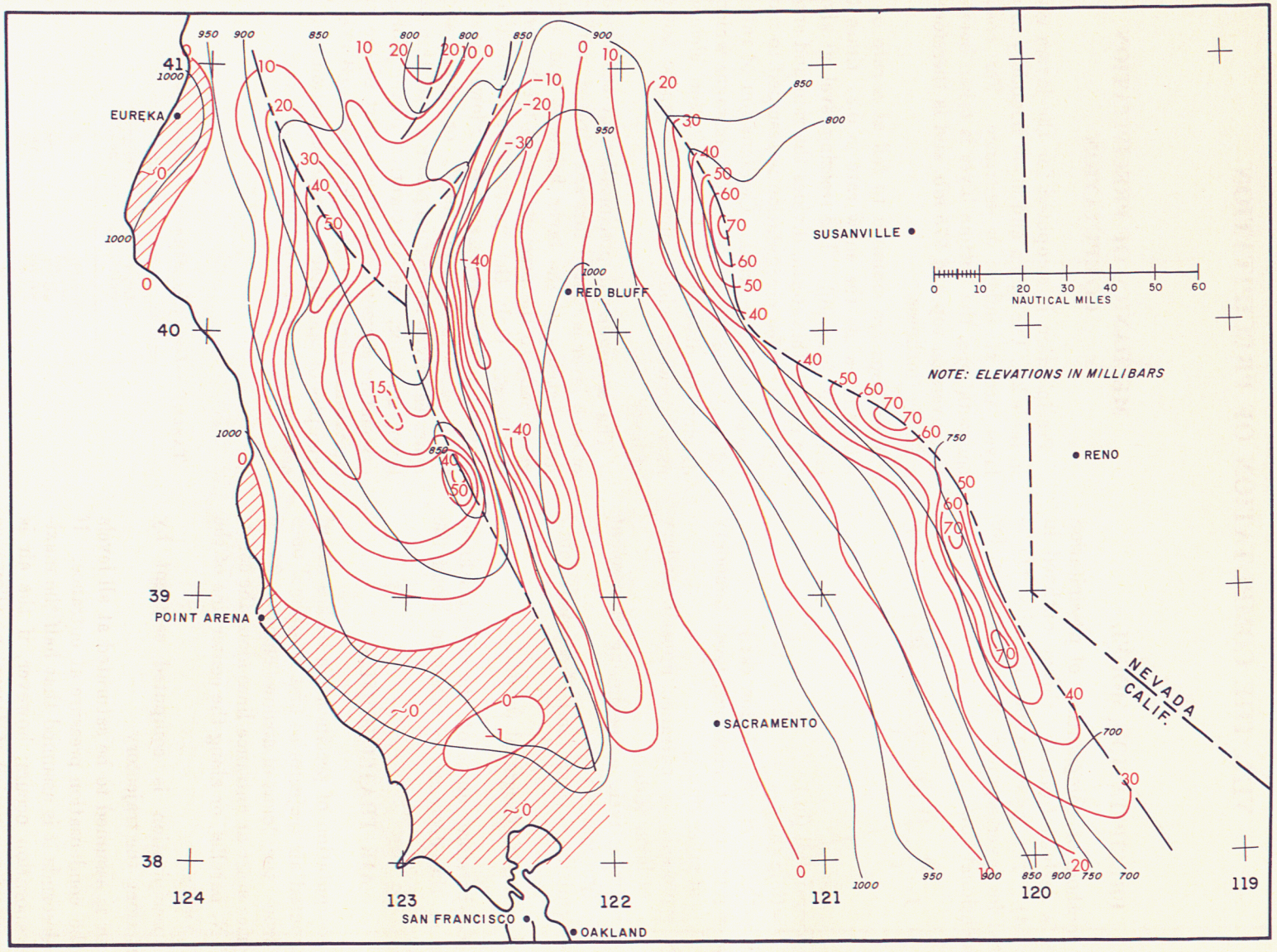

FIGURE 41.—Precipitation rate (units of 0.01 in./6 hr.) calculated for the layer 450–550 mb.

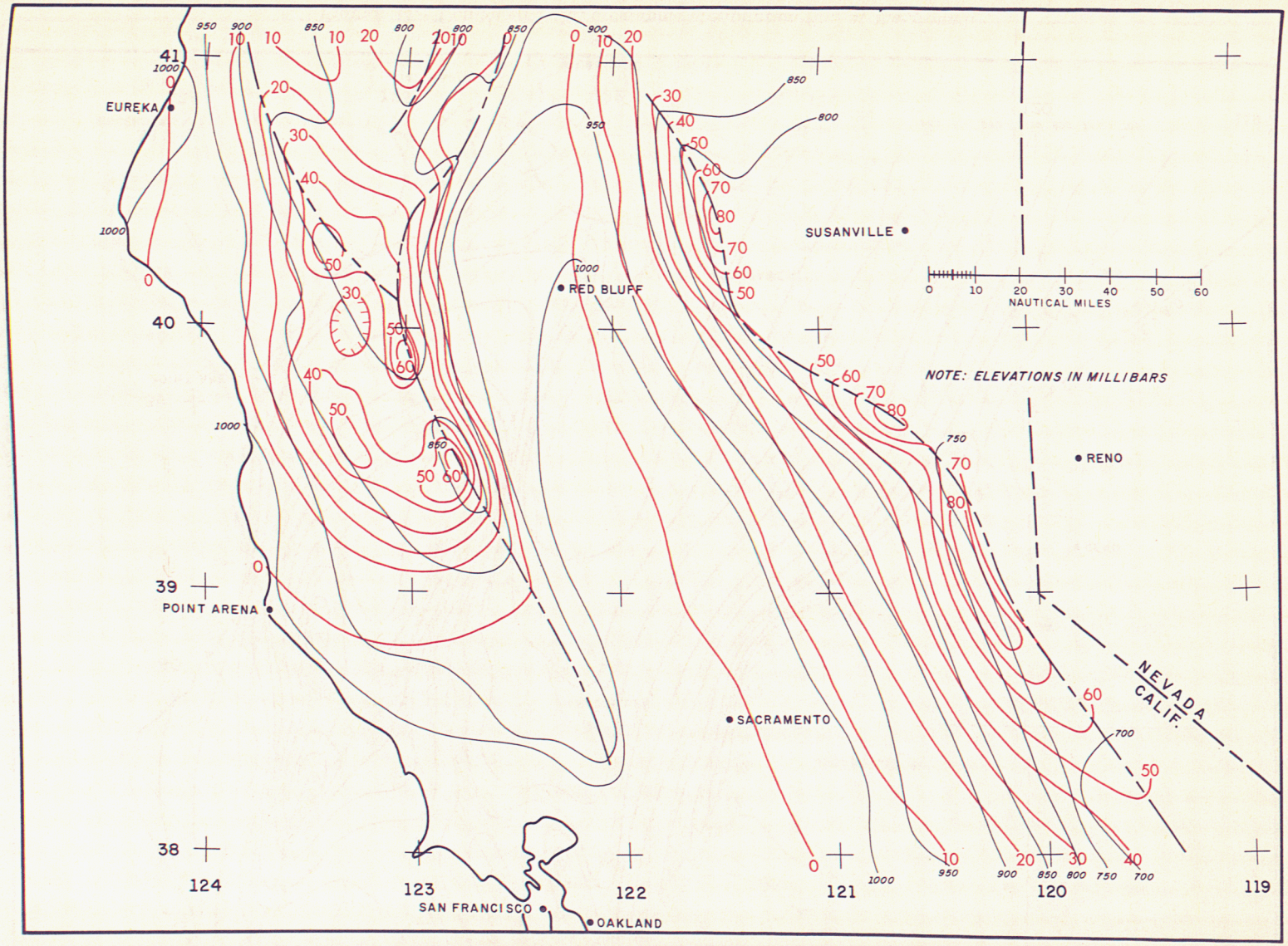

FIGURE 42.—Accumulated precipitation rate (units of 0.01 in./6 hr.) at 550-mb. level.

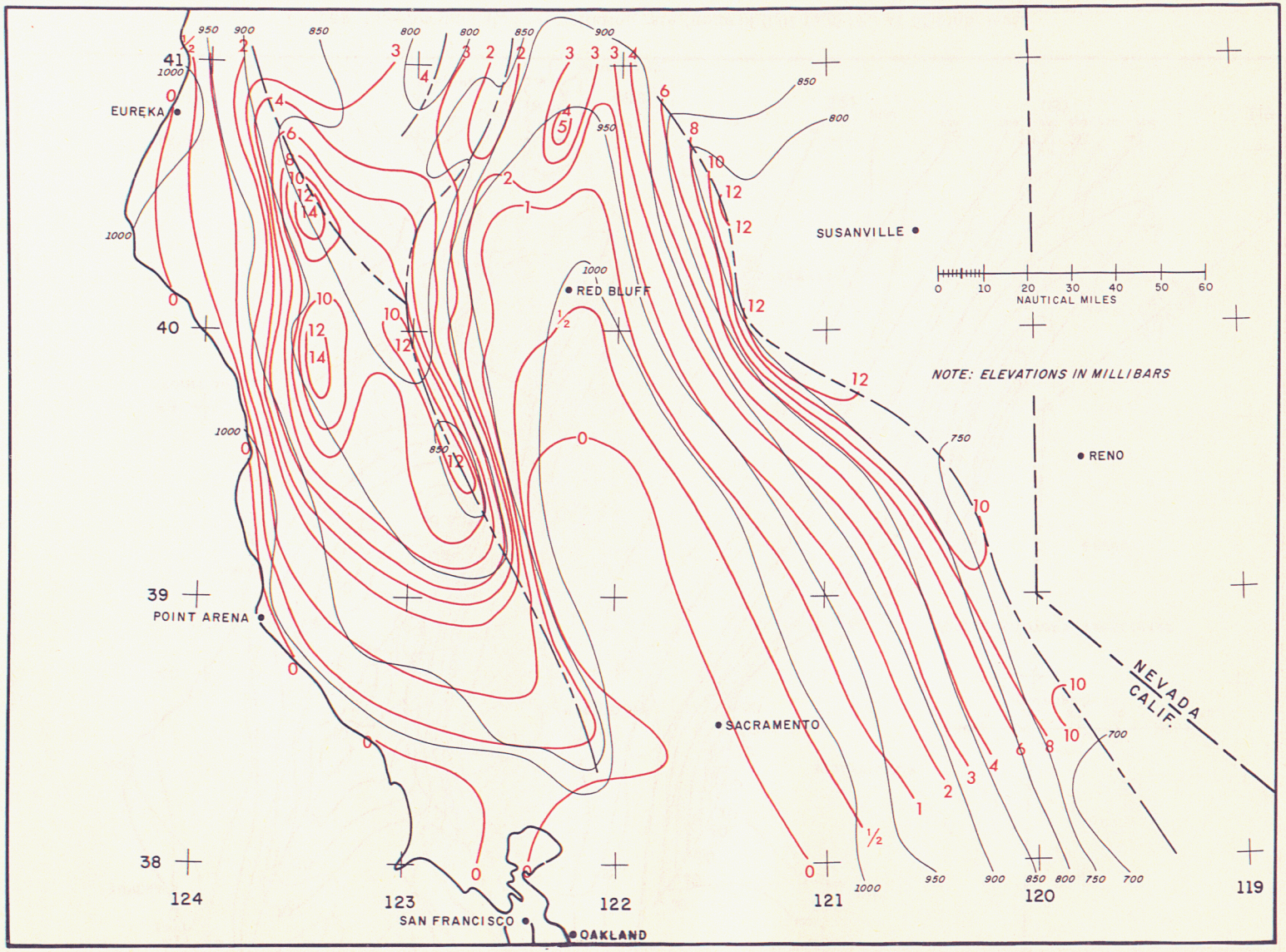

FIGURE 43.—Computed 24-hr. orographic precipitation (in.) at the ground.

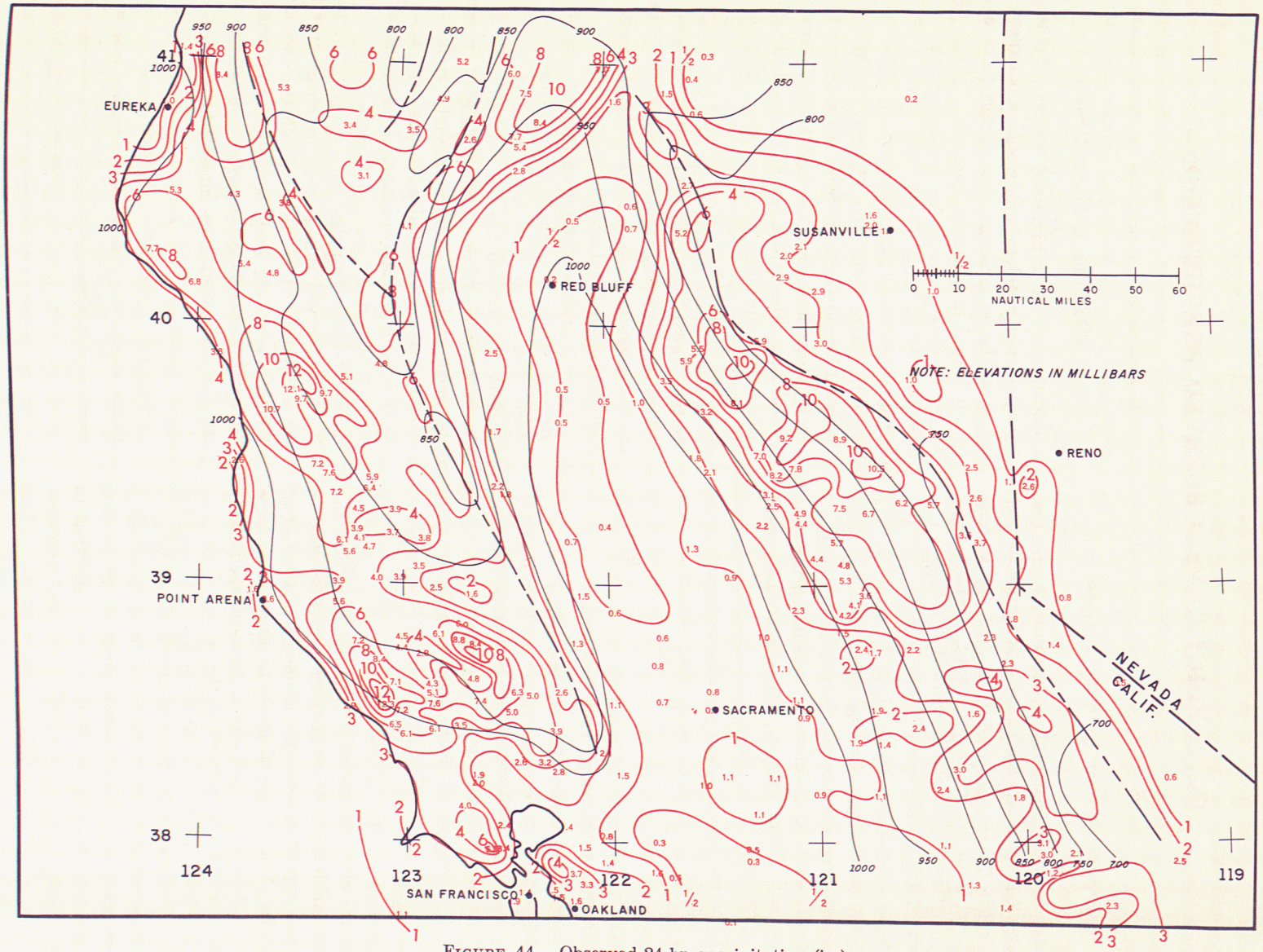

FIGURE 44.—Observed 24-hr. precipitation (in.).

IX. PREDICTED VS. OBSERVED PRECIPITATION

DISTRIBUTION AT THE GROUND

The computed orographic precipitation and the observed precipitation are shown in figures 43 and 44, respectively. The computed, the total accumulated from all the layers above, contains only that portion of the total precipitation which is the result of lift in an assumed laminar flow of air.

The computed precipitation pattern is, in general, similar to the observed, that is, light amounts over the Central Valley and increasing amounts with elevation over the slopes of both the Coast and Sierra ranges, with precipitation centers close to the ridge crests.

Observed precipitation centers occurring over the relatively low ground near the coast are probably due to factors not considered in the present model. They may be due to the release of instability or some frictionally produced eddy phenomena introducing turbulent flow.

On the Sierra slope the observed centers of maximum rainfall are located about 5 to 12 miles from the ridge line, while the computed centers are on or within 5 miles of the ridge line.

The Coast Range is much more "cut up" than the Sierras, and therefore generalization of its topography is more unrealistic. Nevertheless both computed and observed patterns do show maxima close to the main ridge line, except in the most northerly region where the ridge line adopted in this report is more in the nature of the last of a series of nearly equal peaks to air arriving from the southwest. Numerous centers touched off by many ridges are features of the observed precipitation west of the coastal ridge line. Except for one prominent ridge between 40° and 41° N. none of these smaller ridges was used in the streamline constructions and therefore computed rain centers would not usually be formed. An exception to this is the 14-in. center at 39°53′ N. near a concentration of the generalized land contours. (This computed center was verified by a report from Laytonville 3 WNW, 9 n.mi. away, which measured 12.10 in. in the 24-hr. composite period.)

VOLUME COMPARISON

Because of the generalized nature of the approach to the problem, one would not expect the individual heavy precipitation centers to be exactly duplicated in place or amount. The average depth, however, except for non-orographic additions, should be comparable.

The study area was divided into three zones, Coastal, Sierra, and the Central Valley. The "Coastal" region extends from the seacoast to the coastal ridge line; the "Central Valley" from the coastal ridge line to the center line of the Central Valley; and the "Sierra" from the Valley center line to the Sierra ridge line. The Sierra and Coastal are predominantly upslope areas and the Central Valley downslope as defined above.

Average computed and observed precipitation in these zones is given in table 3, together with the average for the total area.

It is seen that the computed amount is an underestimate of the observed precipitation over the Coast Range and the Central Valley. In these areas it is surmised that a net addition to the precipitation is given by convergent processes not accounted for by the model. Spillover of these convergent coastal additions may also contribute to the Valley observed exceedance. In the southern third of the Coastal and Central Valley divisions (roughly between 38° N. and 39° N.) the observed rain is very much greater than the computed, while farther north the exceedance is only slight. It may be conjectured that the low-level southerly or south-southwesterly winds are the important ones in setting off the non-

TABLE 3.—*Average precipitation computed and observed for three zones and the total area*

Area	Computed (inches)	Observed (inches)	C/O
Coastal (upslope)	3.44	4.89	0.70
Central Valley (downslope)	1.12	1.83	0.61
Sierra (upslope)	3.56	2.99	1.19
Total	2.97	3.44	0.86

laminar-flow convective additions, since in the south these winds impinge most strongly upon the coast without first having traveled over significant land features.

Over the Sierras the model overestimates the precipitation by about 20 percent. This may be due in part to a slight drying out of the air because of coastal depletion not as fully compensated by recharge from evaporation as assumed in the model. The deviation from observed conditions is greatest at the northern and southern ends of the Sierra test area, where winds are shielded most from the sea by intervening mountains.

VARIATION OF PRECIPITATION WITH ELEVATION

Attention was next directed to the distribution with elevation of total observed and computed precipitation at the ground. Three areas were chosen for investigation, one along the Sierra and two on the coast. They were selected in regions of the heaviest observed precipitation to illustrate the distribution during very severe conditions. These areas, together with the pattern of precipitation and height, are outlined in figure 45.

Figure 46 shows the results of the investigation. The Sierra comparison illustrates the underestimation on the lower slopes and the reverse at higher elevations mentioned above. The heaviest observed amounts seem to have occurred at about 5500 ft. A decrease with height takes place, to about 3/5 of the maximum value by the 9000-ft. level. The computed rainfall curve, on the other hand, does not peak until about 7000 ft.,

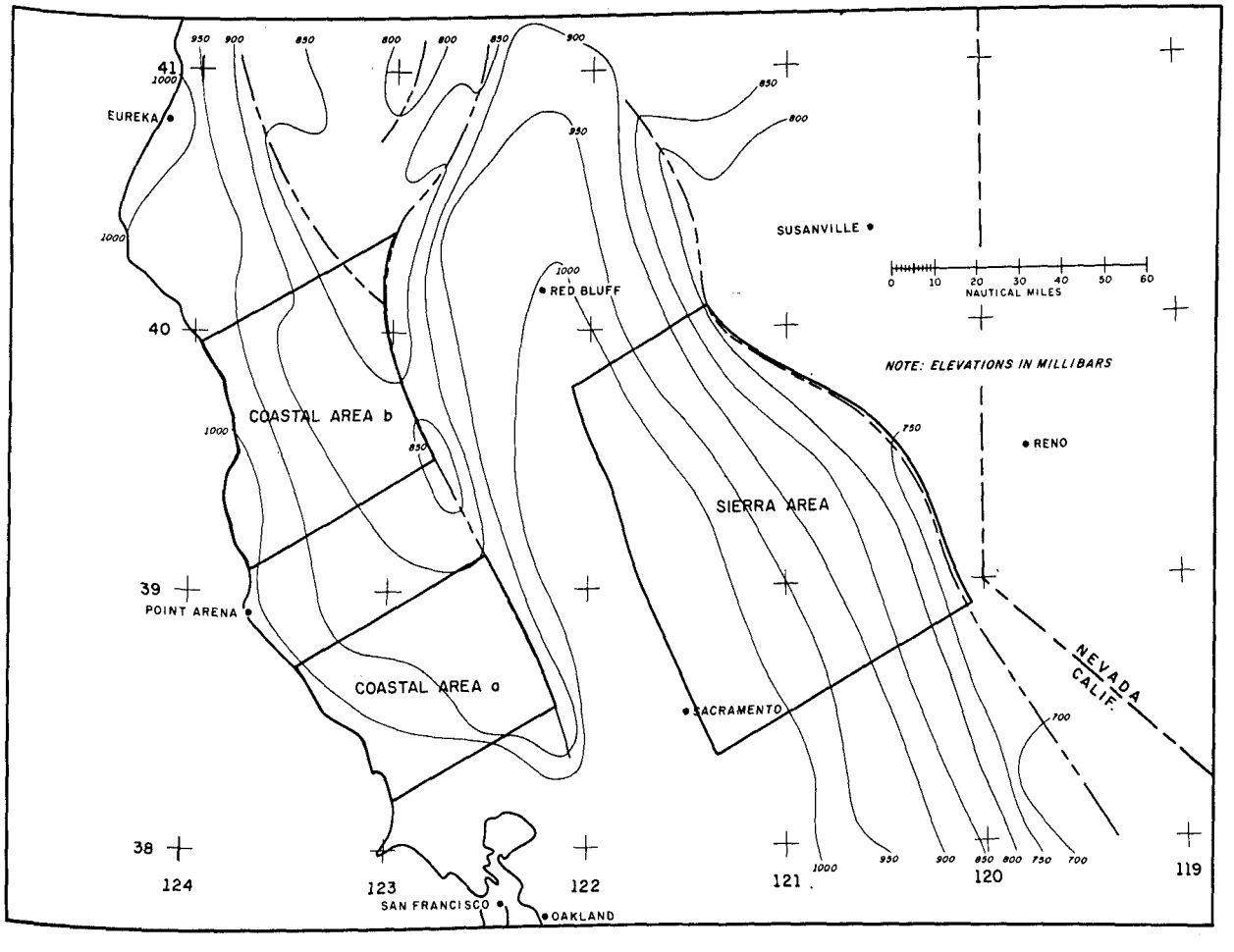

FIGURE 45.—Areas used in comparison of computed and observed precipitation distribution with elevation.

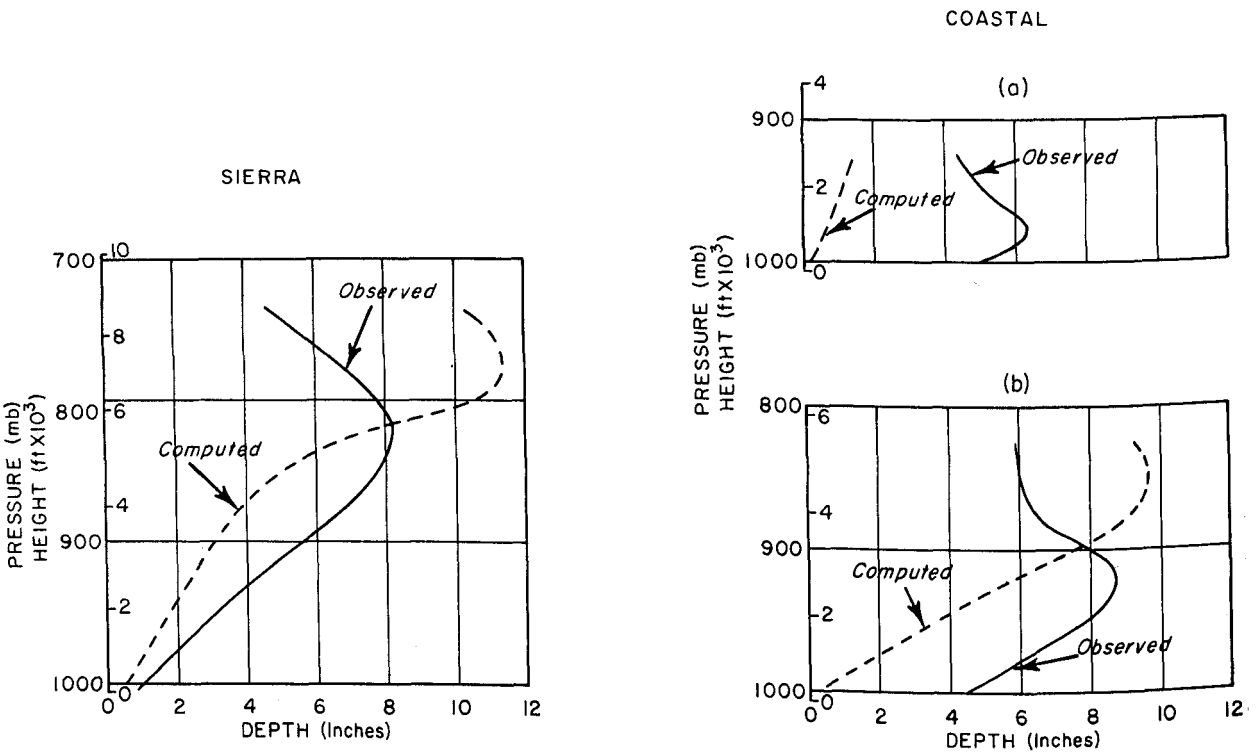

FIGURE 46.—Comparison between computed and observed precipitation amounts in the three areas shown in figure 45.

and the dropoff above this level is much less than that of the observed. It must be remembered, however, that precipitation measurements are very scarce indeed above 6000 ft. (The computed amounts at the upper levels are just as reliable as at the lower elevations.)

The coastal comparisons are also shown on figure 46 (right). The curves for the southern area (a) make clear the very large non-orographic contribution to the total precipitation there. The maximum intensity of this non-orographic rain occurred at about 1000 ft. This particular region must be regarded as somewhat atypical in the December 1955 storm because of its exposure, though the general mechanism is probably common and occurs at some place along the coast in most seacoast storms. The northern area curves (b) resemble those for the Sierra, though non-orographic additions to the precipitation are larger. The observed maximum is at about 3000 ft. while the computed maximum is at about 5000 ft. In this region also observations are very scarce at the higher elevations and the computed precipitation values may be more reliable than the observed.

LAYER CONTRIBUTION TO TOTAL PRECIPITATION

The percentage of the total computed precipitation contributed by each layer is a statistic of interest. Several points (not shown) in the Coastal upslope, the Central Valley, and the Sierra upslope were chosen and the precipitation elements that made up the total at these points were traced back, noting the amount contributed by each layer in the process. It must be borne in mind that the pressure labels of layers are before lift.

A summation of the results of the individual values is shown in figure 47, where Coastal, Central Valley, and Sierra groups are given. Both the Coastal and Sierra rainfall comes from the layer centering about 800 mb., but over the Sierras more of the total precipitation, in terms of percent, comes from this layer. Little or no

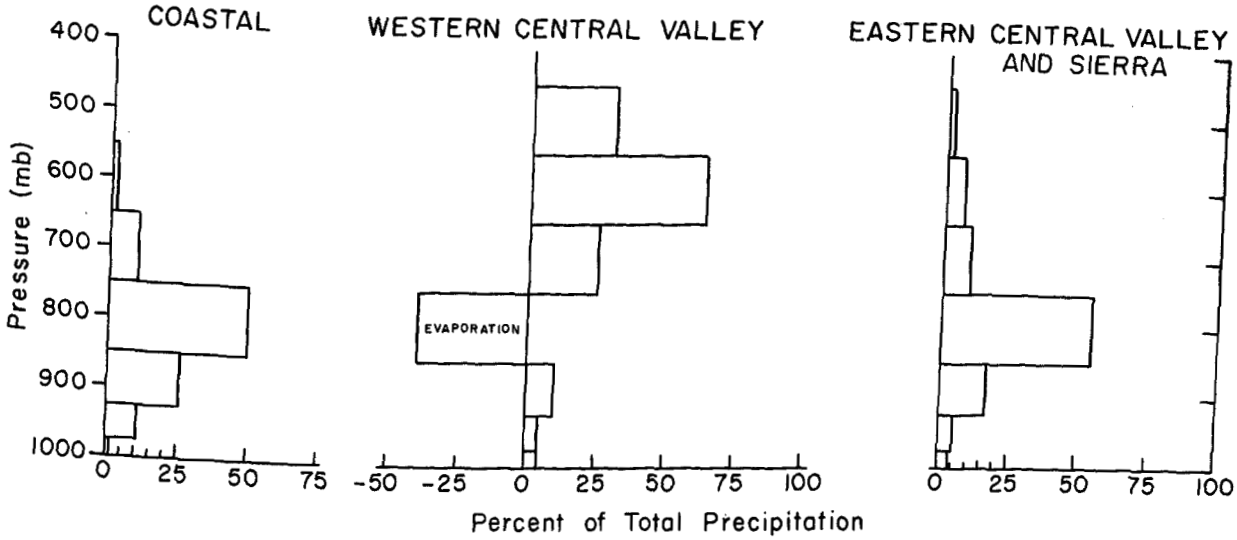

FIGURE 47.—Percentage of total precipitation contributed by each layer.

contribution comes from above 450 mb. and, more surprising, very little comes from below 900 mb. This is due to the relatively low wind speed in the friction layer.

The Central Valley rain, of lower intensity, appears to come from two regions, a very small amount from below 850 mb. and the bulk of the precipitation from about 600 mb. The layer 750–850 mb. actually is an area of negative contribution; i.e., of evaporation.

X. CONCLUSION

This study has attempted to reconstruct over a limited area the three-dimensional distribution of temperature, wind, pressure, and moisture in a major California storm. As partial verification, the precipitation amounts were computed using the appropriate fields and compared with the observed.

Numerically derived temperature soundings were computed for points in the Central Valley and in the mountains, some directly on the highest ridge lines. Computed surface temperatures and pressures, for points where surface observations were taken (Blue Canyon, Red Bluff, and Mt. Shasta) show for the most part very good agreement with observed conditions. Reasonable and consistent temperature soundings were computed for the middle and upper troposphere.

Mesoscale constant pressure charts were derived based on a combination of observed, inferred, and numerically-computed soundings. The charts represent what, in general, must occur on the mesoscale over the mountain ranges in this type of storm. That is, cold troughs are formed by the lifting of stable air and this results in a cross-isobar acceleration of the air toward lower pressure at the center of the trough. This mechanism provides the speed-up needed for the air to pass the barrier.

The three-dimensional wind flow pattern is inferential. Continuity considerations, the observations and extrapolations from them, and the dynamic controls limit the possibilities. Airflow lines between the control points were interpolated. Although there was no direct way to check the total wind flow model, indirectly through the computed precipitation the broadscale adequacy of the model is apparent.

The largest departures from the true three-di-

mensional wind flow undoubtedly occur a few miles inland from the coastline where a band of heavy rainfall was observed but not computed. Elsewhere the quantity and pattern of the orographic precipitation has been duplicated with a good degree of accuracy. Since the region of study is of normal observational density for the type of terrain, it is probable that similar results could be obtained elsewhere. It is also possible that more detail in the precipitation pattern could be captured by (a) closer adherence to the topography, and (b) better input data, preferably from raob reports. Before a complete explanation of the observed precipitation can be obtained, however, account must be taken of the differential frictional barrier at the coastline and the triggering effect of the low hills acting to release instability and to induce large turbulent air motions.

REFERENCES

1. J. Bjerknes, "A Method of Approximate Computation of Orographical Precipitation," Mimeographed report to Corps of Engineers, 1940.
2. Vance A. Myers, "Airflow on the Windward Side of a Large Ridge," *Journal of Geophysical Research*, vol. 67, No. 11, Oct. 1962, pp. 4267–4291.
3. F. Pockels, "The Theory of the Formation of Precipitation on Mountain Slopes," *Monthly Weather Review*, vol. 29, No. 4, Apr. 1901, pp. 152–159. (Translated from *Annalen der Physik*, vol. III, no. 4, 1901, pp. 459–480.)
4. U.S. Weather Bureau, "Preliminary Report on Maximum Possible Precipitation, Los Angeles Area, California," *Hydrometerological Report No. 21A*, 1944, 30 pp.
5. U.S. Weather Bureau, "Maximum Possible Precipitation Over the San Joaquin Basin, California," *Hydrometeorological Report No. 24*, 1947, 93 pp.
6. U.S. Weather Bureau, "Interim Report, Probable Maximum Precipitation in California," *Hydrometeorological Report No. 36*, 1961, 202 pp.
7. U.S. Weather Bureau, "Meteorology of Hydrologically Critical Storms in California, "*Hydrometeorological Report No. 37*, 1962, 207 pp.
8. D. M. Little, "Some Effects of California Mountain Barriers on Upper Air Winds and Sea-Level Isobars," *Monthly Weather Review*, vol. 59, No. 10, Oct. 1931, pp. 376–380.

U.S. GOVERNMENT PRINTING OFFICE: 1963 O—690-385